Geochemistry Geophysics Geosystems G3
AN ELECTRONIC JOURNAL OF THE EARTH SCIENCES
Published by AGU and the Geochemical Society

Article
Volume 1, Number 1
30 May 2000
1009, doi:10.1029/1999GC000020
ISSN: 1525-2027

Age and geochemistry of basaltic complexes in western Costa Rica: Contributions to the geotectonic evolution of Central America

Folkmar Hauff, Kaj Hoernle, and Paul van den Bogaard
GEOMAR Research Center, Wischhofstrasse 1-3, 24148 Kiel, Germany (fhauff@geomar.de)

Guillermo Alvarado
ICE, Departamento Ingeniería Geológica, Apartamento 10032-1000, Costa Rica

Dieter Garbe-Schönberg
Institut für Geowissenschaften der Universität Kiel, Olshausenstrasse 40, 24148 Kiel, Germany

[1] The age and origin of magmatic complexes along the Pacific Coast of Central America have important implications for the origin and tectonic evolution of this convergent plate margin. Here we present new $^{40}Ar/^{39}Ar$ laser age dates, major and trace element data, and initial Sr-Nd-Pb isotope ratios. The 124–109 Ma tholeiitic portions of the Santa Elena complex formed in a primitive island arc setting, believed to be part of the Chortis subduction zone. The geochemical similarities between the Santa Elena and Tortugal alkaline volcanic rocks suggest that Chortis block may extend south of the Hess Escarpment. The Nicoya, Herradura, Golfito, and Burica complexes and the tholeiitic Tortugal unit formed between 95 and 75 Ma and appear to be part of the Caribbean Large Igneous Province, thought to mark the initiation of the Galápagos hotspot. The Quepos and Osa complexes (65–59 Ma) represent accreted sections of an ocean island and an aseismic ridge, respectively, interpreted to reflect part of the Galápagos paleo-hotspot track. An Oligocene unconformity throughout Central America may be related to the mid-Eocene accretion of the Quepos and Osa complexes.

Components: 10,051 words, 8 figures, 6 tables.

Keywords: Central America; oceanic crust; $^{40}Ar/^{39}Ar$-geochronology; geochemistry; plate tectonics; Galápagos hotspot.

Index Terms: 9360 Geographic Location: South America; 8150 Tectonophysics: Plate boundary: general (3040); 4825 Oceanography: Biological and Chemical: Geochemistry; 1708 History of Geophysics: Geochronology.

Received 11 October 1999; **Revised** 18 February 2000; **Accepted** 24 February 2000; **Published** 30 May 2000.

Hauff, F., K. Hoernle, P. van den Bogaard, G. Alvarado, and D. Garbe-Schönberg (2000), Age and geochemistry of basaltic complexes in western Costa Rica: Contributions to the geotectonic evolution of Central America, *Geochem. Geophys. Geosyst.*, *1*, 1009, doi:10.1029/1999GC000020.

1. Introduction

[2] The Pacific margin of Costa Rica contains several oceanic igneous basement complexes that hold key information for reconstructing the origin and tectonic evolution of this convergent plate boundary. The complexes from NW to SE are (1) Santa Elena, (2) Nicoya, (3) Tortugal, (4) Herradura, (5) Quepos, (6) Osa, (7) Golfito, and (8) Burica (Figure 1). Various models have been suggested to explain their magmatic origin and geodynamic setting. These

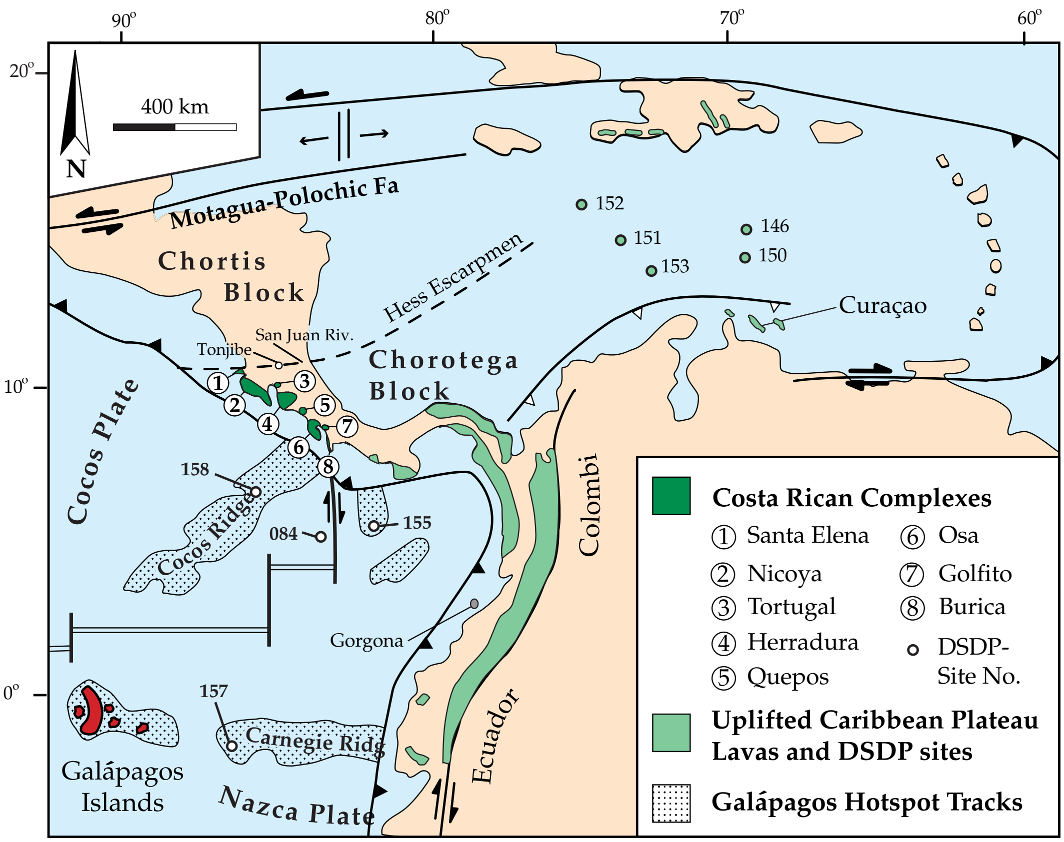

Figure 1. Regional map of Central America, the Caribbean, and northwestern South America showing the studied igneous complexes in Costa Rica, uplifted circum-Caribbean basement, Deep Sea Drilling Project (DSDP) drill sites, the location of the present Galápagos Islands with its hotspot tracks, and the major structural elements of this region. Modified after *Kerr et al*. [1997].

include accretion of Pacific mid-ocean ridge basalt (MORB) crust [*Galli-Olivier*, 1979], accretion of the Galápagos paleo-hotspot track [*Flüh*, 1983], uplift of Caribbean oceanic plateau crust [*Donnelly et al*., 1990; *Duncan and Hargraves*, 1984], and/or a multistage geodynamic evolution beginning with oceanic crust formation at a mid-ocean ridge, followed by intraplate, island arc, and back arc basin volcanism [*Berrangé and Thorpe*, 1988; *Frisch et al*., 1992; *Schmidt-Effing*, 1979]. The longevity of this controversy mainly results from the lack of reliable data on the age and geochemistry of the igneous basement. To date, timing of magmatism has primarily been inferred from biostratigraphic ages of associated sediments, even though contacts between sediments and igneous rocks are predominantly tectonic or intrusive. The majority of earlier radiometric dating studies were conducted on whole rock using the K/Ar analyses method, the application of which is problematic in low-K altered rocks (see *Alvarado et al*. [1992] for a summary). Recent $^{40}Ar/^{39}Ar$ dating of the Nicoya, Herradura, and Quepos complexes in conjunction with geochemical investigations showed that they formed between 92 and 60 Ma from a plume-type mantle source, possibly the Galápagos hotspot [*Hauff et al*., 1997; *Sinton et al*., 1997]. According to these authors, the Nicoya and Herradura complexes mark the westernmost edge of the Caribbean Large Igneous Province (CLIP), while the younger Quepos terrane represents an accreted seamount/ocean island complex of the early Galápagos hotspot track. The age and origin of the other five igneous complexes, however, are poorly constrained. Using laser $^{40}Ar/^{39}Ar$ age dating, major and trace element analyses, and initial Sr-Nd-Pb isotope compositions from all igneous complexes (see Table A1 for sample locations), we propose a geodynamically consistent model for the evolution of the Pacific plate margin of Central America.

2. Sample Preparation and Analytical Methods

[3] Rock chips free of any obvious signs of alteration (veins, crusts, etc.) were picked under a binocular microscope and ground to flour in an agate mortar and agate mill. Volatile contents (H_2O and CO_2) were determined on a Rosemount infrared photometer. Major elements (SiO_2, Al_2O_3, MgO, Fe_2O_3, CaO, Na_2O, K_2O, TiO_2, MnO, and P_2O_5) and trace elements (V, Ni, Cr, Sr, and Zr) were measured on fused beads using a Phillips X'Unique PW1480 X-ray fluorescence spectrometer (XRF) at GEOMAR Research Center. Analytical accuracy and precision (2σ) for Basalt Hawaiian Volcanic Observatory 1 (BHVO-1), and National Bureau of Standards (NBS) 688 lies within ±3% of the working values of *Govindaraju* [1994] for major elements and within ±7% for trace elements at concentration levels >20 ppm. Rb, Ba, Y, Nb, Ta, Hf, U, Th, Pb, and all rare earth elements (REE) were determined with a VG-Plasmaquad PQ1 inductively coupled plasma–mass spectrometer (ICP-MS) at the Geological Institute of the University of Kiel after the methods of *Garbe-Schönberg* [1993]. Relative to the working values of *Govindaraju* [1994] and *Jochum et al*. [1990], BHVO-1, Icelandic basalt 1 (BIR-1), and NBS 688 yielded an analytical accuracy within ±10% for all trace elements and better than ±5% for the REE. Within-run precision is generally better than 2%, and external reproducibility is generally better than 3%. XRF and ICP-MS data are shown in Tables 1 and 2, respectively.

[4] Sr, Nd, and Pb isotope ratios and U-Th-Pb concentrations by isotope dilution analyses were carried out on a Finnigan MAT262-RPQ^{2+} thermal ionization mass spectrometer at GEOMAR and on a Finnigan MAT261 at the Department of Geological Sciences at the University of California in Santa Barbara (UCSB). Analytical results and initial isotope ratios are displayed in Tables 3–5, and the analytical procedures are described by *Hoernle and Tilton* [1991] and *Hauff et al*. [2000]. Errors are reported at the 2σ confidence level. Within-run normalization factors are $^{88}Sr/^{86}Sr = 8.3752$ for $^{87}Sr/^{86}Sr$ and $^{146}Nd/^{144}Nd = 0.7219$ for $^{143}Nd/^{144}Nd$. NBS987 gave $^{87}Sr/^{86}Sr = 0.710247 \pm 6$ ($n = 15$) at GEOMAR and $^{87}Sr/^{86}Sr = 0.710200 \pm 20$ ($n = 12$) at UCSB. Sr isotope data for samples SE27, BC17, GO2, 084-1, 155-1, 157-1, and 158-1 measured at UCSB were normalized to $^{87}Sr/^{86}Sr = 0.710250$ for NBS987. La Jolla yielded $^{143}Nd/^{144}Nd = 0.511847 \pm 4$ ($n = 12$) at GEOMAR, and the AMES standard averaged $^{143}Nd/^{144}Nd = 0.511893 \pm 10$ ($n = 25$) at UCSB, which is in good agreement with the long-term value of $^{143}Nd/^{144}Nd = 0.511889 \pm 9$ obtained at the UCSB laboratory and correlates with a value of 0.51185 for La Jolla (G. R. Tilton, personal communication, 1997). NBS981 gave a fractionation correction of 0.12%/amu for Pb isotope ratios relative to the values of *Todt et al*. [1996] at both GEOMAR and UCSB and was applied to the samples. Replicate analyses of 16 samples give an external reproducibility better

Table 1. XRF Analyses of Igneous Rocks From Oceanic Basement Complexes in Costa Rica[a]

	Rock	Major Elements, wt%														Trace Elements, ppm				
Sample	Type	SiO_2	TiO_2	Al_2O_3	Fe_2O_3	MnO	MgO	CaO	Na_2O	K_2O	P_2O_5	H_2O	CO_2	Total	Mg#	Cr	Ni	V	Sr	Zr
Santa Elena Unit: I																				
SE18	mbs	47.56	2.74	15.48	11.56	0.17	4.99	8.16	4.87	0.96	0.40	3.42	0.04	100.36	51.7	37	40	306	352	214
SE20	dike	39.66	3.56	11.10	13.25	0.45	8.59	15.38	1.49	1.32	0.41	1.82	2.31	99.34	61.6	383	166	402	573	193
SE21	dike	43.81	3.24	15.33	10.45	0.51	4.60	7.62	2.21	5.57	0.84	2.72	2.99	99.88	52.2	70	20	275	392	311
Santa Elena Unit: II, III, IV																				
SE2	gab	49.95	0.17	19.19	4.59	0.09	8.16	14.59	1.74	0.06	0.02	1.70	0.04	100.30	81.5	219	98	159	88	13
SE3	dike	55.96	0.73	15.02	7.89	0.14	6.71	9.65	2.27	0.06	0.04	1.60	0.04	100.11	67.8	61	26	292	108	25
SE6	pbs	51.31	1.18	15.84	10.23	0.18	5.64	8.05	5.18	0.19	0.10	2.50	0.04	100.44	57.7	56	28	275	198	78
SE22a	dike	51.16	1.01	18.52	8.09	0.13	5.09	10.13	4.32	0.13	0.11	1.95	0.03	100.68	60.9	67	39	228	154	75
SE22b	dike	49.75	1.14	16.92	9.03	0.14	6.58	10.42	3.63	0.09	0.11	2.63	0.05	100.49	64.4	60	48	256	176	71
SE24	amph	50.15	1.11	15.62	9.31	0.16	7.14	10.00	3.66	0.13	0.11	3.18	0.03	100.60	65.5	206	66	272	185	72
SE27	dike	53.44	1.25	14.85	10.84	0.18	4.80	8.73	3.79	0.36	0.12	2.51	0.04	100.91	52.3	36	17	329	135	79
SE30	pbs	49.76	1.22	15.60	10.23	0.17	6.95	10.28	3.65	0.16	0.10	2.20	0.12	100.44	62.7	157	65	294	114	71
SE31	dike	49.90	1.38	15.34	11.95	0.18	6.45	8.97	3.81	0.32	0.09	2.50	0.07	100.96	57.2	54	44	400	185	58
SE33	dike	50.21	1.08	15.96	9.76	0.17	7.04	11.41	3.16	0.09	0.08	1.88	0.12	100.97	64.1	129	57	273	131	67
SE34	pbs	51.03	1.13	13.63	13.12	0.20	7.08	10.39	2.38	0.17	0.09	1.46	0.05	100.74	57.2	127	104	362	92	58
Nicoya: Intrusives																				
AN2	gab	49.29	2.06	13.42	16.48	0.25	4.13	7.50	3.74	0.23	0.16	3.56	0.03	100.85	38.3	bdl	bdl	383	211	125
AN14	pgr	70.47	0.54	11.16	7.07	0.13	0.36	4.21	5.46	0.25	0.11	0.84	0.11	100.70	11.2	bdl	bdl	bdl	120	561
BN16	gab	48.80	2.16	13.27	16.33	0.25	4.56	8.44	3.29	0.20	0.15	3.63	0.04	101.13	40.9	24	11	498	187	111
Nicoya: Extrusives																				
BN23	pgr	48.37	1.27	14.39	11.61	0.18	8.06	11.93	2.22	0.22	0.10	2.43	0.11	100.89	63.2	268	110	321	152	68
BN30	gab	49.62	1.16	13.67	13.03	0.20	7.35	10.28	2.33	0.21	0.09	2.76	0.05	100.74	58.3	51	71	343	88	61
BN31	gab	50.46	0.50	16.61	8.36	0.17	7.04	12.24	2.47	0.04	0.02	2.05	0.02	99.99	67.6	18	42	214	130	25
AN3	pbs	48.10	1.63	13.36	14.50	0.23	6.76	10.90	2.03	0.21	0.13	2.29	0.08	100.20	53.6	78	70	392	114	93.5
AN18	mbs	48.73	0.76	13.22	9.73	0.16	10.96	12.92	1.65	0.13	0.05	2.01	0.08	100.39	73.6	890	213	274	71	38
AN21	pbs	49.80	1.22	13.50	12.37	0.22	7.44	10.93	2.26	0.25	0.10	1.73	0.08	99.90	59.9	156	90	382	91.5	63
AN23	pbs	49.66	1.21	13.96	12.44	0.21	7.69	10.79	2.42	0.27	0.10	1.23	0.08	100.06	60.5	155	95	382.5	105.5	62
AN24	mbs	47.25	1.21	13.38	12.78	0.21	7.49	9.48	3.52	0.05	0.10	3.27	0.12	98.86	59.2	181	114	340	126	73
AN28	mbs	49.54	1.03	14.07	11.37	0.19	8.20	11.25	2.25	0.22	0.07	1.78	0.07	100.04	64.1	252	127	318	93	54.5
AN36	bscl	48.82	1.36	13.95	13.94	0.23	7.19	10.82	2.40	0.17	0.10	1.19	0.13	100.27	56.1	104	96	400	81	76
AN46	bscl	48.89	1.80	15.01	11.77	0.20	6.87	10.12	3.25	0.13	0.14	1.02	0.11	99.29	59.1	144	101	424.5	108.5	99.5
AN52	pbs	48.98	0.98	14.00	11.17	0.19	8.33	12.13	2.09	0.23	0.07	1.40	0.18	99.72	64.9	225	132	307	91.5	53

Table 1. (continued)

Sample	Rock Type	Major Elements, wt%												Total	Mg#	Trace Elements, ppm				
		SiO_2	TiO_2	Al_2O_3	Fe_2O_3	MnO	MgO	CaO	Na_2O	K_2O	P_2O_5	H_2O	CO_2			Cr	Ni	V	Sr	Zr
									Nicoya: Extrusives											
AN53	mbs	48.46	0.99	14.22	11.30	0.23	8.63	12.61	1.96	0.05	0.08	0.95	0.13	99.60	65.4	223	136	311.5	76.5	52
AN54	mbs	48.92	0.98	14.26	11.06	0.22	8.58	12.63	1.94	0.07	0.08	1.08	0.21	100.03	65.8	223	131	310.5	79	48
AN56	mbs	48.11	1.41	12.29	13.91	0.22	6.06	10.13	2.16	0.09	0.11	3.26	0.43	98.18	51.9	117	84	371	151	80
AN63	pbcl	48.78	0.99	13.63	11.46	0.20	8.25	11.58	2.15	0.24	0.07	2.03	0.31	99.68	64.1	303	114	305	136	54
AN64	pbscl	49.15	0.97	13.27	11.00	0.18	7.68	10.81	2.58	0.20	0.08	2.89	0.27	99.07	63.4	295	109	309	162	48
AN71	mbs	48.46	0.98	13.82	11.31	0.20	8.61	11.21	2.75	0.16	0.07	2.14	0.14	99.83	65.4	298	139	308	144.5	50.5
AN72	bsc	49.46	0.96	14.31	10.76	0.19	8.23	11.52	2.29	0.31	0.07	1.80	0.10	99.98	65.5	276	125	302	126	54
AN75	pbs	48.93	0.91	13.99	10.72	0.19	8.83	12.09	2.10	0.21	0.08	2.33	0.14	100.52	67.1	282	118	295	244	44.5
AN76	mbs	48.72	0.75	14.38	10.17	0.16	8.66	12.19	1.87	0.34	0.05	2.00	0.06	99.35	67.9	296	136	261	82	41
AN81	pbs	48.89	0.96	13.95	11.42	0.22	8.96	11.93	2.14	0.16	0.07	1.38	0.08	100.14	66.0	291	132	314.5	95	52.5
AN86	mbscl	49.48	2.42	13.12	15.27	0.23	5.63	8.86	2.68	0.14	0.22	1.35	0.09	99.48	47.7	76	68	544	102	146.5
AN87	pbs	48.96	0.76	14.28	10.12	0.16	8.69	12.24	1.94	0.34	0.05	3.93	0.46	101.92	68.0	345	138	269	82	40
AN99	pbs	48.98	0.99	14.01	10.84	0.31	8.63	11.66	2.59	0.16	0.07	1.55	0.23	100.02	66.4	281	123	318	73	55
AN102	pbscl	49.25	0.99	13.89	10.89	0.35	8.41	10.41	3.26	0.25	0.07	2.11	0.13	99.98	65.7	298	128	325.5	74	54
AN108	pbs	46.78	0.96	13.14	11.15	0.18	7.53	11.26	1.57	0.18	0.07	3.84	0.18	96.84	62.6	212	127	289	207	41
AN110	pbs	48.65	1.00	13.86	11.45	0.19	8.41	12.13	1.84	0.10	0.08	1.79	0.16	99.67	64.5	306	106	310.5	107.5	53.5
AN119	mbs	48.67	1.62	13.33	14.60	0.24	7.08	10.60	2.73	0.28	0.13	1.60	0.05	100.94	54.6	106	71	392	120	86
AN121	mbs	48.55	1.63	13.20	14.71	0.23	6.68	10.56	2.54	0.15	0.13	2.54	0.07	100.99	53.0	72	57	397	112	88
AN123	mbs	48.53	1.61	13.34	14.75	0.23	6.51	10.52	2.71	0.27	0.14	1.50	0.04	100.16	52.2	89	71	404	125	92
AN124	pbs	49.06	1.03	15.30	9.94	0.17	8.23	11.37	2.80	0.25	0.09	2.38	0.08	100.69	67.2	307	131	292	115	55
AN125	mbs	49.45	1.09	14.11	11.38	0.19	7.79	10.74	2.88	0.14	0.09	2.45	0.05	100.36	62.9	302	114	322	276	54
AN126	mbs	49.02	1.25	13.74	13.38	0.21	7.42	9.25	3.39	0.37	0.12	2.89	0.08	101.12	57.9	98	85	361	130	65
AN127	pbscl	48.37	2.33	12.46	17.77	0.24	4.42	8.74	3.24	0.21	0.19	2.82	0.07	100.86	38.1	28	30	516	237	124
AN128	mbs	49.98	0.80	13.59	9.97	0.19	8.71	10.11	3.42	0.24	0.06	2.96	0.08	100.11	68.4	365	126	264	377	38
BN10	mbs	49.14	0.85	14.25	9.90	0.15	8.16	12.26	1.62	0.61	0.05	3.42	0.28	100.70	67.1	395	128	274	85	43
BN14	mbs	47.84	0.83	14.21	10.69	0.17	8.11	12.22	2.37	0.46	0.06	2.63	0.43	100.01	65.3	377	129	274	113	43
BN17	pbs	49.75	1.61	12.74	14.28	0.21	6.34	8.81	2.68	1.46	0.13	2.08	0.08	100.17	52.4	62	58	386	80	91
BN19	pbs	50.16	0.88	14.73	9.52	0.17	8.60	12.75	1.86	0.16	0.07	1.55	0.06	100.51	69.1	376	156	273	87	47
BN20	pbs	48.91	1.68	13.30	14.75	0.22	6.19	10.38	2.67	0.13	0.15	2.65	0.09	101.11	51.0	75	54	396	114	93
BN21	pbs	49.44	1.00	14.08	11.06	0.18	7.95	11.65	2.29	0.07	0.08	3.01	0.12	100.93	64.1	241	103	306	208	50
BN22	pbs	49.02	1.26	14.51	11.65	0.17	7.90	12.33	2.31	0.11	0.10	1.54	0.24	101.14	62.7	253	104	323	111	65
BN26	pbs	48.79	1.66	13.15	14.81	0.24	6.71	10.36	2.64	0.16	0.13	1.96	0.04	100.65	52.9	75	55	399	127	91
BN29	mbs	48.03	1.44	14.92	12.38	0.18	5.56	10.53	2.58	0.15	0.11	5.11	0.07	101.06	52.7	33	37	341	459	76
BN33	pbs	46.14	1.14	13.30	11.71	0.21	7.24	11.48	3.06	0.44	0.09	1.55	4.10	100.47	60.5	196	103	325	265	60

Table 1. (continued)

Sample	Rock Type	Major Elements, wt%												Total	Mg#	Trace Elements, ppm				
		SiO_2	TiO_2	Al_2O_3	Fe_2O_3	MnO	MgO	CaO	Na_2O	K_2O	P_2O_5	H_2O	CO_2			Cr	Ni	V	Sr	Zr
Herradura																				
AH1a	mbs	48.15	1.05	13.79	11.27	0.16	8.24	11.63	1.75	0.06	0.07	1.88	0.14	98.19	64.4	345	124	327	316	47
AH1b	mbs	48.58	1.08	14.23	11.25	0.17	8.55	12.20	1.87	0.06	0.08	1.68	0.13	99.88	65.3	393	122	321	227.5	53.5
AH2	pbs	49.03	1.07	13.93	10.96	0.17	8.87	12.02	1.90	0.04	0.07	2.14	0.17	100.37	66.7	377	129	321	92.5	56
AH4	pbs	48.76	1.03	13.78	10.89	0.19	8.75	12.04	2.01	0.06	0.08	2.16	0.31	99.40	66.6	407	139	308.5	90.5	53.5
AH5	pbs	47.92	2.28	16.24	11.75	0.17	5.81	8.94	3.66	0.58	0.21	3.43	0.07	101.06	55.1	74	50	333	328	138
AH6	pbs	49.15	1.07	13.83	11.04	0.19	9.13	11.79	2.22	0.08	0.07	2.42	0.17	101.16	67.2	433	144	312	93	54
AH8	pbs	49.35	0.84	14.46	10.24	0.16	8.87	11.55	2.12	0.28	0.06	2.48	0.12	100.53	68.2	400	140	281	395	41
BH11	mbs	48.73	0.88	14.44	10.33	0.18	9.43	11.77	2.29	0.08	0.07	2.19	0.10	100.48	69.4	437	167	280	105	46
Tortugal: Alkaline Series																				
TG1	pic	41.27	0.70	4.47	12.21	0.17	28.75	4.61	0.34	0.12	0.07	6.29	0.24	99.24	85.4	2189	1573	152	85	52
TG2	pic	42.36	0.59	4.98	11.41	0.17	27.98	5.20	0.42	0.37	0.07	5.70	0.19	99.43	85.9	2846	1564	156	378	24
TG3	pic	41.35	0.80	4.44	11.28	0.16	27.84	4.80	0.17	0.07	0.07	7.11	0.30	98.39	86.0	2393	1585	143	69	54
TG4	pic	42.03	0.66	4.74	11.51	0.17	28.89	4.91	0.29	0.09	0.06	5.85	0.20	99.39	86.2	2543	1606	143	95	47
TG5	bs	42.02	0.62	5.22	11.24	0.16	26.24	5.15	0.06	0.02	0.05	7.35	0.28	98.41	85.3	2447	1385	148	35	39
TG6	bs	49.23	3.22	12.96	13.22	0.20	6.24	6.76	3.67	0.69	0.27	3.04	0.37	99.87	53.9	273	181	409	230	197
TG7	bs	36.45	0.85	12.68	10.08	0.15	7.71	11.78	3.30	1.12	0.07	6.58	6.69	97.47	65.5	362	129	269	59	51
TG15	bs	48.69	2.04	14.96	10.77	0.16	5.88	7.80	3.21	2.61	0.22	2.45	0.24	99.03	57.5	54	85	352	1328	96
TG8	bs	48.35	1.41	13.16	14.22	0.16	5.19	8.68	3.67	1.95	0.10	2.01	0.37	99.27	47.5	188	148	205	255	75
TG9	bs	49.49	1.79	12.24	11.83	0.18	7.05	7.86	3.45	2.18	0.17	2.26	0.24	98.75	59.6	452	183	299	383	125
TG10	dike	45.70	2.67	14.74	11.04	0.15	7.26	7.15	2.57	3.23	0.35	3.37	0.49	98.71	62.0	38	47	368	376	231
TG11	dike	48.20	2.60	12.93	12.24	0.16	7.27	7.68	4.32	0.72	0.27	2.81	0.37	99.57	59.6	294	167	337	393	173
TG12	dike	48.16	2.43	11.98	12.53	0.15	7.98	7.90	2.97	1.84	0.25	3.06	0.21	99.46	61.2	712	286	337	656	140
Tortugal: Tholeiitic Series																				
TG13	gab	48.95	0.91	13.81	11.23	0.18	8.65	9.51	2.96	0.44	0.07	2.92	0.13	99.76	65.6	381	156	300	172	50
TG14	gab	47.99	0.84	16.31	10.16	0.18	6.67	8.78	3.51	0.81	0.08	3.61	0.16	99.10	61.9	154	56	290	313	36
BC16	mbs	47.13	3.85	13.28	13.62	0.18	6.32	10.36	2.11	0.35	0.36	2.50	0.10	100.17	53.5	200	125	401	457	249
BC17	mbs	50.48	1.00	13.61	11.38	0.20	7.97	9.60	3.78	0.04	0.09	2.36	0.21	100.71	63.5	268	119	309	155	53
BC18	mbs	49.64	1.02	13.91	11.45	0.18	7.86	9.80	3.25	0.69	0.08	2.74	0.07	100.69	63.0	179	127	327	258	53
Golfito																				
GO1	mbs	56.37	1.29	13.56	13.81	0.18	3.20	5.27	4.37	0.45	0.17	1.85	0.14	100.66	36.5	bdl	bdl	308	149	111
GO2	mbs	51.99	0.98	14.49	11.94	0.17	5.98	6.42	5.27	0.41	0.12	3.10	0.06	100.94	55.4	23	33	268	202	70

Table 1. (continued)

Sample	Rock Type	Major Elements, wt%														Trace Elements, ppm				
		SiO_2	TiO_2	Al_2O_3	Fe_2O_3	MnO	MgO	CaO	Na_2O	K_2O	P_2O_5	H_2O	CO_2	Total	Mg#	Cr	Ni	V	Sr	Zr
									Golfito											
GO3	mbs	50.97	0.76	14.38	10.70	0.18	7.07	7.73	4.65	0.39	0.08	3.08	0.12	100.10	62.1	78	41	277	229	47
GO4	mbs	48.62	1.21	13.71	11.89	0.19	8.17	11.25	2.73	0.22	0.09	2.50	0.09	100.67	63.0	271	117	313	147	65
GO5	mbs	50.92	1.14	15.14	12.63	0.16	5.47	7.08	4.30	0.30	0.14	3.21	0.12	100.60	51.8	21	36	396	164	63
									Burica											
BUR4	bs	48.49	0.89	14.21	10.45	0.16	8.54	11.87	2.56	0.11	0.07	1.88	0.03	99.39	66.95	390	128	291	166	47
BUR5	bs	48.93	0.85	14.49	10.17	0.16	8.77	12.61	1.93	0.11	0.06	1.51	0.03	99.74	68.13	384	121	288	93	46
BUR11	bs	47.97	1.13	14.43	10.91	0.20	8.40	12.05	2.81	0.10	0.09	2.15	0.19	100.57	65.62	319	122	293	148	59
BUR12	bs	49.03	1.24	13.81	12.24	0.20	8.25	9.84	3.56	0.38	0.09	2.78	0.07	101.71	62.56	219	96	317	140	62
BUR13	bs	47.96	1.43	14.37	11.97	0.21	7.11	12.16	2.79	0.10	0.12	1.88	0.03	100.24	59.55	76	61	359	157	76
BUR14	bs	48.26	1.18	13.42	11.80	0.17	7.76	10.46	3.70	0.15	0.09	3.03	0.03	100.18	61.98	208	86	318	170	63
									Quepos Intrusives											
AQ22	gab	49.38	2.43	15.03	10.87	0.18	5.99	10.03	2.53	1.31	0.23	1.12	0.08	99.18	57.7	120	46	255	141	43
BQ28	gab	52.59	0.65	15.10	9.76	0.16	6.81	10.37	2.50	0.44	0.06	2.29	0.06	100.79	63.4	41	22	350	107	68
BQ31b	gab	52.28	0.93	14.44	11.98	0.19	5.71	9.93	2.39	0.11	0.11	2.01	0.08	100.15	54.2	32	24	314	114	56
BQ31a	gab	52.60	0.65	15.09	9.74	0.16	6.76	10.37	2.54	0.44	0.07	2.16	0.05	100.62	63.2	125	48	264	142	45
BQ32	gab	52.65	1.12	14.04	13.02	0.21	5.24	8.88	3.01	0.28	0.13	1.69	0.11	100.38	49.9	41	22	350	107	68
BQ72	gab	48.30	1.89	13.85	13.20	0.27	7.14	8.54	3.71	0.51	0.18	2.33	0.03	99.95	57.3	115	58	345	161	129
									Quepos Extrusives											
AQ8	bs	47.21	2.71	13.87	12.62	0.30	7.18	11.22	2.41	0.46	0.27	1.01	0.16	99.42	58.5	295	130	383	264	157
AQ10	bscl	47.33	2.75	13.55	12.81	0.22	6.65	9.70	3.34	0.67	0.26	2.39	0.09	99.76	56.3	227	142	419	365	157
AQ16	pbs	47.21	2.28	13.05	12.88	0.18	8.66	10.99	2.24	0.24	0.18	1.39	0.11	99.40	62.5	750	303	324	218	123
AQ19	pbs	47.82	2.73	13.84	12.48	0.19	7.21	11.02	2.52	0.39	0.24	1.22	0.12	99.78	58.9	338	162	356	272	165
AQ20	bdcl	46.66	2.39	13.08	12.29	0.18	8.41	10.71	2.73	0.52	0.21	1.89	0.34	99.41	62.9	504	234	309	215	131
AQ23	bs	46.95	2.88	13.26	13.00	0.36	6.89	9.77	3.42	0.53	0.27	2.43	0.14	99.90	56.8	246	120	404	207	173
AQ28	pic	42.44	1.22	6.16	12.61	0.16	27.76	4.65	0.96	0.13	0.11	3.52	0.08	99.80	84.5	1643	1462	161	91	75
AQ32	bs	43.91	1.51	9.25	13.65	0.17	15.64	6.08	1.88	0.32	0.13	5.74	0.19	98.47	74.0	1528	1091	216	133	89
AQ39	bscl	42.72	2.58	14.71	14.60	0.17	6.15	8.33	3.73	1.30	0.24	5.51	0.44	100.48	51.1	84	113	341	255	171
AQ41	bs	47.50	2.82	13.98	12.49	0.20	5.67	9.25	3.69	0.96	0.26	2.80	0.07	99.69	52.9	153	119	342	627	149
AQ43	pbs	47.72	2.56	13.61	12.47	0.20	7.28	10.54	3.02	0.23	0.23	1.71	0.08	99.65	59.1	334	146	359	241	149
AQ43b	bs	47.09	2.63	13.15	12.76	0.21	7.10	9.83	3.76	0.41	0.25	2.55	0.13	99.86	58.0	321	133	377	192	156
AQ49	bscl	45.64	2.87	12.98	13.45	0.27	7.01	9.82	3.30	0.74	0.29	2.87	0.62	99.86	56.4	286	145	399	192	175

Table 1. (continued)

Sample	Rock Type	Major Elements, wt%														Trace Elements, ppm				
		SiO_2	TiO_2	Al_2O_3	Fe_2O_3	MnO	MgO	CaO	Na_2O	K_2O	P_2O_5	H_2O	CO_2	Total	Mg#	Cr	Ni	V	Sr	Zr
								Quepos Extrusives												
AQ55	pic	43.45	1.37	7.70	12.55	0.17	24.01	5.74	1.16	0.25	0.12	3.38	0.17	100.07	82.6	1684	1123	189	125	80
AQ62	bscl	47.26	2.38	13.88	11.98	0.26	7.27	12.18	2.42	0.44	0.20	1.43	0.12	99.82	60.1	462	196	341	272	138
AQ66	bs	48.03	2.89	13.64	12.76	0.19	6.83	10.43	2.80	0.48	0.26	1.02	0.05	99.38	57.0	304	142	375	295	174
BQ70	bs	48.94	2.26	13.67	11.54	0.17	6.59	9.90	3.78	0.55	0.20	2.19	0.33	100.13	58.6	198	87	332	341	131
BQ71	bs	47.24	2.25	13.96	11.96	0.17	6.64	10.49	3.70	0.27	0.18	2.89	0.10	99.85	57.9	213	101	338	340	129
AQ72	bscl	48.69	2.22	13.81	11.70	0.15	6.26	9.93	4.33	0.14	0.20	2.57	0.09	100.09	57.0	201	96	338	286	119
								Osa												
OS2	mbs	48.51	1.34	14.25	12.88	0.28	7.38	12.35	1.85	0.05	0.09	1.76	0.05	100.79	58.7	162	80	331	104	74
OS4	pbs	49.10	1.26	14.26	10.52	0.21	8.44	11.51	2.63	0.19	0.10	2.80	0.24	101.26	66.5	298	106	327	166	69
OS6	pbs	50.12	1.02	14.85	10.78	0.18	6.49	11.11	3.11	0.49	0.08	2.22	0.05	100.50	59.9	117	53	307	110	54
OS9	mbs	49.15	0.89	13.51	10.04	0.16	10.63	11.00	1.97	0.10	0.07	3.29	0.08	100.88	72.4	583	249	272	102	48
OS16	mbs	46.26	1.13	15.75	10.72	0.20	8.89	13.51	1.77	0.16	0.09	2.25	0.12	100.84	67.3	341	120	268	148	70
								DSDP Leg 14/16												
84-1	bs	49.26	1.09	15.77	9.43	0.16	7.01	12.65	2.38	0.17	0.09	1.61	0.12	99.74	64.8	377	100	273	113	74
155-1	bs	54.26	2.04	16.94	5.69	0.07	5.81	3.83	2.48	6.01	0.31	2.35	0.66	100.45	71.7	182	103	200	239	158
155-4	bs	48.43	1.97	17.32	8.76	0.12	7.39	7.23	3.47	1.11	0.30	3.04	0.99	100.13	67.7	175	79	207	412	145
157-1	bs	47.49	2.23	15.05	11.36	0.33	6.85	9.36	3.23	0.29	0.20	2.18	0.18	98.75	59.9	219	58	380	210	145
157-2	bs	48.29	2.25	14.81	11.74	0.25	7.62	9.33	3.04	0.15	0.20	1.78	0.18	99.64	61.7	213	53	390	202	140
157-4	bs	47.73	2.06	13.79	12.10	0.17	7.33	10.76	2.81	0.13	0.19	1.37	0.12	98.55	60.0	200	49	355	177	130
157-5	bs	49.11	2.06	13.75	12.48	0.21	6.59	11.50	2.63	0.18	0.19	0.91	0.22	99.83	56.7	214	47	346	174	137
157-6	bs	46.92	2.11	13.43	12.96	0.23	6.58	11.51	2.64	0.20	0.18	1.21	0.28	98.25	55.7	198	47	352	176	132
158-1	bs	48.80	1.89	15.09	11.48	0.12	7.88	8.73	2.99	0.15	0.19	2.31	0.15	99.78	63.0	137	54	366	222	114
								Standards												
NBS688	*N* = 20	48.64	1.21	17.40	10.37	0.17	8.49	12.26	2.00	0.19	0.14	n.d.	n.d.	100.9	n.d.	314	137	243	169	56
	±2σ	0.30	0.01	0.12	0.04	0.002	0.06	0.06	0.07	0.01	0.01	-	-	0.47	-	7.19	7.00	8.47	3.57	3.75
BHVO-1	*N* = 17	49.75	2.78	13.56	12.33	0.17	7.14	11.27	2.09	0.52	0.27	-	-	99.89	-	290	133	283	398	159
	±2σ	0.33	0.02	0.15	0.10	0.002	0.09	0.08	0.12	0.01	0.01	-	-	0.56	-	9.09	16.76	26.31	6.40	9.49

[a]Here amph, amphibolite; gab, gabbro; pgr, plagiogranite; pic, picrite; bs, basalt; pbs, pillow basalt; cl, clast; mbs, massive basalt.

Table 2. Trace Element Data From Costa Rican Igneous Basement Complexes[a]

Sample	Rock Type	Trace Elements, ppm																						
		Ba	Rb	Hf	Nb	Ta	Y	Pb	Th	U	La	Ce	Pr	Nd	Sm	Eu	Gd	Tb	Dy	Ho	Er	Tm	Yb	Lu
St. Elena: II–IV																								
SE2	gab	13	0.35	0.26	0.08	0.01	5.2	0.12	0.02	0.01	0.25	0.66	0.12	0.77	0.37	0.18	0.60	0.12	0.92	0.21	0.60	0.10	0.63	0.10
SE3	dike	19	0.67	0.80	0.21	0.02	12.4	0.30	0.05	0.03	0.79	2.42	0.46	2.64	1.10	0.45	1.63	0.32	2.22	0.49	1.41	0.21	1.48	0.22
SE06	pbs	77	3.12	2.03	0.94	0.07	25.6	0.24	0.09	0.05	2.22	7.54	1.38	7.52	2.75	0.98	3.66	0.69	4.61	0.98	2.83	0.42	2.83	0.42
SE27	dike	77	3.54	1.95	1.19	0.09	25.3	0.62	0.16	0.08	2.76	8.31	1.46	7.75	2.79	1.01	3.73	0.70	4.68	1.00	2.83	0.43	2.83	0.42
St. Elena: I																								
SE20	dike	453	27.69	5.78	43.98	2.68	19.5	2.30	4.06	1.07	35.48	74.07	9.31	37.91	7.78	2.34	6.57	0.93	4.66	0.82	1.95	0.25	1.51	0.21
Nicoya																								
AN2	gab	83	3.35	2.22	7.23	0.49	44.8	0.14	0.42	0.10	7.12	17.80	2.70	13.36	4.38	1.58	5.60	0.99	6.26	1.31	3.77	0.55	3.60	0.54
AN3	pbs	21	3.62	2.49	5.07	0.34	36.5	0.49	0.36	0.12	4.77	12.47	1.93	9.80	3.36	1.20	4.43	0.79	5.09	1.09	3.16	0.46	3.09	0.46
AN14	pgr	84	3.78	1.36	21.15	1.45	143.8	0.23	1.01	0.22	16.77	47.26	7.53	38.07	12.59	3.63	15.89	2.95	19.58	4.20	12.72	1.97	14.42	2.28
AN18	mbs	35	3.41	0.93	2.09	0.14	16.6	0.23	0.13	0.04	1.81	4.72	0.74	3.99	1.43	0.55	1.95	0.36	2.39	0.53	1.57	0.23	1.50	0.23
AN23	pbs	12	1.34	1.70	4.11	0.28	27.2	0.33	0.29	0.09	3.12	8.27	1.30	6.71	2.34	0.87	3.22	0.60	4.12	0.91	2.75	0.40	2.72	0.40
AN28	mbs	37	1.48	1.45	3.37	0.23	21.3	0.22	0.25	0.07	2.78	7.16	1.10	5.71	1.94	0.73	2.68	0.49	3.26	0.71	2.13	0.32	2.14	0.32
AN46	bscl	36	1.44	3.36	5.81	0.39	44.8	0.51	0.48	0.19	6.28	17.09	2.69	13.50	4.54	1.61	5.80	1.05	6.64	1.40	4.05	0.58	3.87	0.56
AN52	pbs	11	1.94	1.41	2.97	0.20	22.4	0.26	0.23	0.07	2.58	6.68	1.03	5.30	1.88	0.72	2.62	0.47	3.06	0.68	2.05	0.31	2.00	0.30
AN53	mbs	6	0.32	1.36	3.04	0.21	20.5	0.26	0.22	0.07	2.50	6.53	1.04	5.41	1.85	0.71	2.57	0.48	3.17	0.69	2.07	0.30	2.04	0.30
AN63	pbcl	18	1.74	1.47	3.10	0.21	21.7	0.23	0.23	0.08	2.74	7.03	1.10	5.77	1.99	0.74	2.70	0.49	3.30	0.73	2.18	0.31	2.14	0.32
AN72	bsc	16	3.82	1.39	3.29	0.23	20.0	0.31	0.25	0.08	2.48	6.71	1.07	5.44	1.87	0.71	2.57	0.47	3.12	0.68	2.07	0.29	1.97	0.30
AN76	mbs	24	2.27	0.99	2.13	0.15	15.5	0.16	0.15	0.06	1.96	5.08	0.80	4.07	1.42	0.55	1.94	0.36	2.43	0.53	1.59	0.23	1.57	0.22
AN81	pbs	7	1.40	1.23	2.88	0.20	21.1	0.24	0.20	0.07	2.44	6.41	1.01	5.20	1.86	0.70	2.54	0.46	3.12	0.67	2.01	0.29	1.97	0.30
AN86	mbscl	35	1.55	3.95	9.06	0.62	55.6	0.74	0.62	0.20	6.78	19.31	3.00	15.16	5.12	1.72	6.65	1.18	7.70	1.66	4.96	0.72	4.82	0.73
AN99	pbs	28	1.51	1.41	3.16	0.21	23.3	0.29	0.24	0.08	2.84	7.42	1.16	6.00	2.01	0.75	2.75	0.50	3.29	0.72	2.15	0.31	2.07	0.30
AN110	pbs	19	1.11	1.39	3.11	0.22	21.2	0.22	0.25	0.08	2.67	6.93	1.08	5.68	1.92	0.73	2.62	0.49	3.28	0.71	2.13	0.31	2.05	0.31
AN119	mbs	23	2.72	2.39	4.83	0.32	32.4	0.48	0.33	0.13	4.53	11.86	1.86	9.43	3.17	1.15	4.19	0.77	5.09	1.08	3.17	0.46	3.06	0.45
AN123	mbs	22	3.12	2.41	5.15	0.35	33.5	0.49	0.34	0.12	4.76	12.56	1.98	9.84	3.30	1.22	4.33	0.79	5.25	1.11	3.26	0.46	3.13	0.45
AN124	pbs	42	2.12	1.21	3.41	0.23	19.3	0.30	0.21	0.07	2.95	7.47	1.15	5.72	1.88	0.73	2.49	0.46	3.04	0.64	1.86	0.27	1.79	0.26
AN125	mbs	237	1.70	0.75	3.69	0.25	21.6	0.13	0.19	0.05	3.33	8.31	1.26	6.35	2.05	0.78	2.77	0.51	3.38	0.72	2.08	0.30	1.98	0.29
AN126	mbs	382	7.01	1.52	4.13	0.29	24.8	0.17	0.27	0.11	4.19	10.28	1.56	7.64	2.45	0.92	3.30	0.59	3.87	0.83	2.43	0.35	2.35	0.35
AN127	mbs	55	3.68	1.97	7.26	0.50	41.3	0.15	0.28	0.07	6.86	18.04	2.79	14.00	4.54	1.66	5.78	1.05	6.77	1.39	4.00	0.56	3.65	0.54
BN17	pbs	85	12.27	2.33	5.10	0.31	28.4	0.10	0.34	0.11	4.34	11.61	1.87	9.46	3.22	1.16	4.28	0.77	5.17	1.06	3.01	0.45	2.95	0.44
BN19	pbs	11	2.28	1.15	2.47	0.15	15.8	0.24	0.15	0.08	2.02	5.45	0.87	4.45	1.58	0.60	2.20	0.41	2.76	0.59	1.69	0.26	1.74	0.26

Table 2. (continued)

Sample	Rock Type	Trace Elements, ppm																						
		Ba	Rb	Hf	Nb	Ta	Y	Pb	Th	U	La	Ce	Pr	Nd	Sm	Eu	Gd	Tb	Dy	Ho	Er	Tm	Yb	Lu
Herradura																								
BN31	gab	9	0.21	0.44	0.93	0.06	9.2	0.08	0.05	0.01	0.88	2.38	0.41	2.16	0.84	0.42	1.21	0.24	1.66	0.35	1.00	0.15	1.01	0.15
AH1b	mbs	28	0.99	1.44	3.96	0.27	22.9	0.33	0.24	0.08	3.22	8.04	1.22	5.95	2.01	0.74	2.70	0.48	3.18	0.69	2.07	0.31	2.02	0.30
AH5	pbs	36	8.71	1.68	3.88	0.27	27.4	0.39	0.27	0.10	3.59	9.08	1.42	7.07	2.40	0.89	3.22	0.61	4.13	0.90	2.65	0.39	2.61	0.39
AH8	pbs	23	1.50	1.13	2.39	0.21	15.3	0.20	0.15	0.05	1.90	5.06	0.82	4.19	1.50	0.59	2.10	0.40	2.72	0.58	1.65	0.25	1.69	0.26
BH11	mbs	24	0.69	1.20	2.88	0.17	15.3	0.21	0.19	0.06	2.43	6.32	1.00	4.96	1.67	0.63	2.30	0.42	2.85	0.60	1.71	0.26	1.73	0.26
Tortugal																								
TG4	pic	82	3.69	1.08	6.21	0.39	6.2	1.04	0.43	0.14	5.09	10.75	1.40	6.04	1.42	0.48	1.48	0.22	1.36	0.27	0.69	0.10	0.62	0.09
TG6	bs	149	14.69	5.00	23.17	1.55	32.3	1.67	1.68	0.53	18.77	43.83	6.05	26.76	6.95	2.28	6.92	1.07	5.98	1.11	2.85	0.37	2.25	0.31
TG8	bs	433	24.66	2.10	8.86	0.61	19.2	1.81	0.60	0.11	8.18	18.71	2.60	11.51	3.07	1.04	3.29	0.52	3.14	0.64	1.80	0.25	1.58	0.23
TG9	bs	761	38.70	3.31	24.83	1.67	21.8	3.78	2.22	0.59	24.93	45.52	5.39	21.00	4.59	1.42	4.37	0.64	3.70	0.71	1.95	0.27	1.76	0.26
TG10	dike	748	29.51	5.90	37.62	2.47	29.7	2.14	3.87	1.06	36.96	79.84	9.92	39.54	8.17	2.38	7.03	0.97	5.30	0.99	2.68	0.36	2.32	0.33
TG11	dike	90	8.57	4.37	32.64	2.02	27.3	1.66	2.04	0.67	28.48	58.03	7.20	29.18	6.37	2.12	6.19	0.90	4.94	0.92	2.42	0.32	1.98	0.28
TG12	dike	1732	17.21	3.96	29.20	1.82	26.2	2.26	1.85	0.60	26.30	51.97	6.51	26.57	5.95	1.92	5.99	0.84	4.72	0.87	2.28	0.30	1.83	0.26
TG13	gab	109	6.21	1.41	3.00	0.21	22.1	0.57	0.24	0.07	3.12	7.90	1.21	6.16	2.11	0.78	2.77	0.50	3.39	0.73	2.17	0.32	2.12	0.31
BC-17	mbs	22	0.24	1.58	3.02	0.19	19.4	0.25	0.22	0.08	2.71	7.48	1.21	6.17	2.17	0.79	2.85	0.54	3.54	0.78	2.21	0.33	2.25	0.34
Golfito																								
GO1	mbs	120	6.61	3.09	4.67	0.28	36.0	0.31	0.64	0.22	5.83	14.65	2.28	11.09	3.73	1.21	4.89	0.94	6.42	1.41	4.16	0.66	4.42	0.68
GO2	mbs	96	6.85	1.85	2.96	0.19	24.2	0.19	0.27	0.06	4.09	9.88	1.55	7.65	2.47	0.85	3.41	0.65	4.33	0.96	2.71	0.41	2.76	0.42
GO4	mbs	19	3.26	1.79	3.59	0.23	21.0	0.34	0.23	0.08	2.97	8.22	1.36	6.90	2.40	0.91	3.21	0.58	3.86	0.79	2.23	0.33	2.20	0.33
Burica																								
BUR4	bs	44	1.28	1.27	2.66	0.16	16.7	0.18	0.18	0.06	2.35	6.13	0.99	5.10	1.76	0.68	2.39	0.45	3.00	0.66	1.81	0.28	1.84	0.28
BUR13	bs	110	0.89	2.19	3.78	0.24	24.8	0.12	0.27	0.10	3.44	9.74	1.62	8.47	2.89	1.08	3.89	0.70	4.59	0.97	2.64	0.41	2.62	0.39
Quepos																								
AQ8	bs	64	4.64	4.10	14.76	0.99	30.4	0.71	0.96	0.38	11.47	28.12	4.08	18.95	5.19	1.76	5.74	0.92	5.35	1.05	2.86	0.37	2.35	0.33
AQ16	pbs	35	2.74	3.20	12.12	0.83	23.5	0.63	0.72	0.27	8.58	21.43	3.12	14.62	3.99	1.40	4.45	0.73	4.25	0.83	2.27	0.30	1.86	0.27
AQ19	pbs	77	5.88	4.24	15.67	1.06	31.0	0.61	1.02	0.35	12.06	30.17	4.37	20.00	5.47	1.82	6.08	0.94	5.50	1.08	2.92	0.39	2.48	0.34
AQ20	bscl	64	9.92	3.45	13.47	0.90	29.5	0.68	0.85	0.28	10.79	26.88	3.73	17.40	4.66	1.60	5.17	0.81	4.65	0.92	2.44	0.32	2.01	0.29
AQ22	gab	97	22.26	3.98	15.74	1.05	27.1	0.60	1.11	0.38	12.84	30.31	4.23	19.29	5.04	1.67	5.45	0.86	4.96	0.95	2.56	0.33	2.05	0.29
AQ43	pbs	58	3.02	3.72	14.11	0.93	31.6	0.64	0.88	0.29	10.52	26.83	3.78	17.92	4.81	1.64	5.46	0.87	5.13	1.01	2.75	0.38	2.27	0.33
AQ62	bscl	58	3.96	3.92	13.30	0.89	29.7	0.68	0.90	0.27	10.93	27.23	3.94	18.23	5.02	1.67	5.51	0.89	5.24	1.04	2.89	0.38	2.43	0.34
AQ72	bscl	18	2.54	3.17	11.80	0.77	31.9	0.78	0.81	0.42	10.43	24.44	3.48	16.47	4.34	1.52	5.14	0.83	4.91	1.01	2.76	0.38	2.44	0.35

Table 2. (continued)

Sample	Rock Type	Trace Elements, ppm																						
		Ba	Rb	Hf	Nb	Ta	Y	Pb	Th	U	La	Ce	Pr	Nd	Sm	Eu	Gd	Tb	Dy	Ho	Er	Tm	Yb	Lu
Quepos																								
BQ32	gab	53	3.28	1.70	2.93	0.17	27.0	0.21	0.27	0.10	3.65	9.36	1.49	7.53	2.68	0.94	3.59	0.70	4.78	1.07	3.00	0.47	3.19	0.49
BQ72	gab	104	5.00	3.70	4.15	0.27	39.1	1.18	0.34	0.11	5.19	15.17	2.54	13.45	4.67	1.72	6.06	1.12	7.34	1.55	4.24	0.65	4.19	0.61
AQ28	pic	25	2.18	1.77	7.16	0.42	11.7	0.32	0.45	0.15	5.39	13.08	1.89	8.44	2.29	0.77	2.48	0.39	2.35	0.44	1.14	0.16	0.99	0.14
Osa																								
OS02	mbs	13	0.41	2.05	3.64	0.25	23.6	0.42	0.26	0.09	3.44	9.47	1.57	7.92	2.80	1.03	3.71	0.69	4.54	0.96	2.66	0.40	2.67	0.39
OS06	pbs	14	11.53	1.46	0.48	0.03	24.5	0.18	0.05	0.06	1.00	3.61	0.76	4.58	2.03	0.80	3.13	0.60	4.28	0.92	2.66	0.41	2.72	0.41
OS09	mbs	6	1.00	1.22	2.66	0.26	15.3	0.27	0.19	0.07	2.25	5.91	0.95	4.75	1.66	0.60	2.24	0.41	2.81	0.59	1.75	0.25	1.68	0.25
OS16	mbs	17	0.99	1.43	2.72	0.82	23.6	0.08	0.14	0.03	2.32	7.05	1.25	6.69	2.44	0.92	3.41	0.62	4.28	0.90	2.62	0.37	2.44	0.35
DSDP Leg14/16																								
84-1	bs	3	3.76	1.99	0.96	0.06	24.8	1.74	0.09	0.06	2.06	7.07	1.29	7.20	2.60	1.00	3.62	0.66	4.53	0.99	2.84	0.44	2.87	0.43
155-1	bs	241	27.15	3.93	19.69	1.17	20.4	0.90	1.41	1.24	11.14	25.12	3.47	15.69	4.07	1.39	4.47	0.74	4.34	0.84	2.22	0.30	1.90	0.26
157-5	bs	35	2.87	3.66	9.32	0.61	31.6	0.68	0.69	0.23	8.06	20.76	3.12	15.12	4.42	1.57	5.46	0.97	6.22	1.29	3.47	0.51	3.33	0.47
158-1	bs	46	0.62	3.23	10.18	0.64	25.0	0.73	0.89	0.39	8.44	20.44	2.92	13.74	4.01	1.44	4.71	0.82	5.08	1.04	2.83	0.40	2.57	0.38
Standards																								
NBS 688	$N = 7$	172.38	2.05	1.59	3.80	0.26	18.33	2.69	0.32	0.28	5.09	11.68	1.71	8.13	2.37	0.96	2.91	0.52	3.40	0.74	2.07	0.31	2.09	0.32
	$\pm 2\sigma$	5.25	0.10	0.05	0.12	0.01	0.62	0.48	0.02	0.04	0.19	0.41	0.04	0.19	0.06	0.04	0.07	0.02	0.13	0.02	0.07	0.02	0.07	0.01
BHVO-1	$N = 5$	132.31	9.58	4.61	16.96	1.09	23.70	1.92	1.20	0.42	15.19	36.95	5.27	23.84	6.01	2.01	6.06	0.94	5.30	0.97	2.43	0.33	1.99	0.28
	$\pm 2\sigma$	1.94	0.26	0.10	0.51	0.02	0.66	0.09	0.05	0.02	0.25	0.64	0.10	0.41	0.17	0.04	0.09	0.03	0.11	0.03	0.06	0.01	0.06	0.01
BIR-1	$N = 25$	5.99	0.18	0.58	0.51	0.04	13.89	3.46	0.03	0.01	0.58	1.74	0.35	2.14	1.02	0.48	1.70	0.34	2.45	0.53	1.62	0.23	1.57	0.24
	$\pm 2\sigma$	0.57	0.03	0.01	0.04	0.002	0.35	0.21	0.00	0.01	0.004	0.11	0.02	0.13	0.05	0.01	0.04	0.01	0.04	0.01	0.02	0.01	0.03	0.004

[a]Here gab, gabbro; pgr, plagiogranite; pic, picrite; bs, basalt; pbs, pillow basalt; cl, clast; mbs, massive basalt; bdl, below detection limit. Asterisk denotes element concentrations determined by XRF from Table 1.

Table 3. Sr Isotope Data From Costa Rican Igneous Basement Complexes[a]

Sample	Age, Ma	Rb, ppm	Sr, ppm	$^{87}Rb/^{86}Sr$	$^{87}Sr/^{86}Sr_m$ Unleached	±2σ	$^{87}Sr/^{86}Sr_m$ Leached	±2σ	$^{87}Sr/^{86}Sr_{in}$ Unleached	$^{87}Sr/^{86}Sr_{in}$ Leached
Santa Elena										
SE2	120	0.35	88	0.012	0.704730	(14)	0.704680	(8)	0.704710	0.704660
SE3	120	0.67	108	0.018	0.704447	(7)	0.704089	(8)	0.704417	0.704059
SE6	120	3.12	198	0.046	0.703210	(10)			0.703132	
SE27	120	3.54	135	0.076	0.703062	(11)	0.703035	(7)	0.702933	0.702906
SE20	120	27.69	573	0.140	0.703735	(7)			0.703497	
Nicoya										
AN2	90	3.35	211	0.046	0.703300	(9)			0.703241	
AN14	90	3.78	120	0.091	0.704264	(8)	0.704185	(8)	0.704148	0.704069
AN18	90	3.41	71	0.139	0.703558	(8)	0.703310	(9)	0.703381	0.703133
AN46	90	1.44	109	0.038	0.703280	(7)			0.703231	
AN52	90	1.94	92	0.061	0.703334	(7)			0.703256	
AN53	90	0.32	77	0.012			0.703025	(6)		0.703010
AN72	90	3.82	126	0.088	0.705779	(7)	0.703208	(7)	0.705667	0.703096
AN81	90	1.40	95	0.043	0.704906	(8)	0.703142	(7)	0.704851	0.703087
AN86	90	1.55	102	0.044	0.703484	(7)			0.703428	
AN99	90	1.51	73	0.060	0.703722	(7)	0.703236	(8)	0.703646	0.703160
AN110	90	1.11	108	0.030	0.703425	(7)			0.703387	
BN17	90	12.27	80	0.438	0.703835	(8)	0.703754	(11)	0.703268	0.703187
BN19	90	2.28	87	0.076			0.703240	(8)		0.703143
BN31	90	0.21	130	0.005	0.703066	(5)			0.703060	
Herradura										
AH5	85	8.71	328	0.077	0.704889	(7)	0.703428	(8)	0.704796	0.703335
AH8	85	1.50	395	0.011	0.703538	(8)	0.703207	(9)	0.703525	0.703194
BH11	85	0.69	105	0.019	0.703627	(7)	0.703846	(8)	0.703604	0.703823
Tortugal										
TG4	90	3.69	95	0.112	0.703636	(8)	0.703518	(7)	0.703492	0.703374
TG8	90	24.66	255	0.280	0.703789	(9)	0.703813	(9)	0.703431	0.703455
TG9	90	38.70	383	0.292	0.704096	(8)			0.703722	
TG13	90	6.21	172	0.104	0.704119	(8)			0.703986	
BC17	90	0.24	155	0.004	0.706200	(8)	0.706344	(8)	0.706194	0.706338
Golfito										
GO1	80	6.61	149	0.128	0.704511	(7)	0.704405	(7)	0.704365	0.704259
GO2	80	6.85	202	0.098	0.705212	(11)	0.705152	(10)	0.705101	0.705041
GO4	80	3.26	147	0.064			0.703667	(7)		0.703594
Burica										
BUR4	80	1.28	166	0.022	0.704194	(8)	0.704203	(8)	0.704169	0.704178
BUR11	80	*1.10*	148	*0.024*	0.703823	(8)			0.703799	
BUR12	80	*1.10*	140	*0.024*	0.703825	(8)			0.703799	
BUR13	80	0.89	157	0.016	0.703443	(9)			0.703424	
BUR14	80	*1.10*	170	*0.024*	0.704042	(7)			0.704021	
Quepos										
AQ8	60	4.64	264	0.051	0.703380	(8)			0.703337	
AQ16	60	2.74	218	0.036	0.703523	(9)			0.703492	
AQ19	60	5.88	272	0.063	0.703344	(9)			0.703291	
AQ22	60	22.26	271	0.238	0.703474	(7)			0.703272	
AQ28	60	2.18	91	0.063	0.703455	(7)			0.703396	

Table 3. (continued)

Sample	Age, Ma	Rb, ppm	Sr, ppm	$^{87}Rb/^{86}Sr$	$^{87}Sr/^{86}Sr_m$ Unleached	±2σ	$^{87}Sr/^{86}Sr_m$ Leached	±2σ	$^{87}Sr/^{86}Sr_{in}$ Unleached	$^{87}Sr/^{86}Sr_{in}$ Leached
					Quepos					
AQ43	60	3.02	241	0.036	0.703994	(7)	0.703141	(8)	0.703963	0.703110
BQ32	60	3.28	107	0.089	0.703488	(8)			0.703412	
					Osa					
OS2	60	0.41	104	0.011	0.703012	(8)	0.702996	(8)	0.703002	0.702986
OS6	60	11.53	110	0.298	0.704491	(8)	0.704380	(7)	0.704233	0.704122
OS9	60	1.00	102	0.028	0.704312	(8)	0.703829	(10)	0.704288	0.703805
OS16	60	0.99	148	0.019	0.703489	(8)	0.703156	(7)	0.703473	0.703140
					DSDP Leg14/16					
					Coiba Ridge					
155-1	20	27.15	239	0.329	0.704971	(5)	0.703554	(10)	0.704878	0.703461
					Carnegie Ridge					
157-5	5	2.87	174	0.048	0.703290	(6)	0.703020	(12)	0.703287	0.703017
					Cocos Ridge					
158-1	10	0.62	222	0.008	0.704420	(8)	0.703376	(7)	0.704419	0.703375
					Cocos Plate					
084-1	20	3.76	113	0.096	0.702996	(11)	0.702532	(44)	0.702969	0.702505

[a] Rb concentrations from ICP–MS, Sr concentrations from XRF, leaching procedure: 50:50 mix of hot 6 NHCI and 6 $NHNO_3$ for 60 min. Errors refer to the least significant digit and are 2σ mean within run precision. When available, initial $(^{87}Sr/^{86}Sr)_{in}$ ratios were calculated from leached $(^{87}Sr/^{86}Sr)_m$ data. Total chemistry blanks were <0.3 ng for Pb, <0.2 ng for Sr, <0.06 ng for Nd, Th, U and thus negligible. The external reproducibility of U-Th-Pb concentration determinations by isotope dilution is better than 1% based on 16 samples while those for Sm-Nd by ICP–MS are <2% and Rb-Sr by ICP–MS and XRF respectively are <4%.

than ±0.000015 for $^{87}Sr/^{86}Sr$, better than ±0.000012 for $^{143}Nd/^{144}Nd$, and better than ±0.03%/amu for Pb isotope ratios.

[5] The $^{40}Ar/^{39}Ar$ laser dating was carried out by total fusion of single plagioclase crystals and basalt matrix fragments (0.1–2 mg) using a 25-W Spectraphysics Argon Ion laser connected to a Mass Analyzer Product (MAP) 216 noble gas mass spectrometer at the GEOMAR Geochronology Laboratory. Plagioclase was leached in 5% HF acid for 15 min and cleaned ultrasonically. Matrix chips were ultrasonically washed in distilled water. All samples were irradiated for 144 hours in the 5-MW reactor at the GKSS Research Center in Geesthacht (Germany), monitor crystals Taylor Creek rhyolite (TCR) sanidine (Batch 85G003, 27.92 Ma [*Duffield and Dalrymple*, 1990]) and samples were mounted in aluminum sample holders for vertical and lateral control of the neutron flux gradients. Vertical variations of the *J* value are corrected through fitting a cosine function to the data after *Bogaard* [1995]. Isotope ratios are corrected for system blanks, mass discrimination, and interfering neutron reactions. Up to 11 crystals or particles for each sample were analyzed, and the results are displayed in $^{36}Ar/^{40}Ar$ versus $^{39}Ar/^{40}Ar$ isotope correlation diagrams (Figure 3). Least squares regressions fitted through the individual data points [*York*, 1969] yield isochrons with mean squared weighted deviates (MSWD) less than 3 and initial $^{40}Ar/^{36}Ar$ ratios that are identical to atmospheric values ($^{40}Ar/^{36}Ar = 295.5$) within 2σ uncertainties, except for one-matrix samples (AN86), which yield lower than atmo-

Table 4. Nd Isotope Data From Costa Rican Igneous Basement Complexes[a]

Sample	Age, Ma	Sm, ppm	Nd, ppm	$^{147}Sm/^{144}Nd$	$^{143}Nd/^{144}Nd_m$	±2σ	$^{143}Nd/^{144}Nd_{in}$	εNdt
				Santa Elena				
SE2	120	0.37	0.77	0.293	0.513215	(16)	0.512985	9.78
SE3	120	1.10	2.64	0.251	0.513163	(19)	0.512966	9.42
SE6	120	2.75	7.52	0.220	0.513160	(7)	0.512987	9.82
SE27	120	2.79	7.75	0.217	0.513134	(23)	0.512964	9.37
SE20	120	7.78	37.91	0.123	0.512733	(7)	0.512636	2.97
				Nicoya				
AN2	90	4.38	13.36	0.197	0.513015	(5)	0.512899	7.35
AN14	90	12.59	38.07	0.199	0.513021	(3)	0.512904	7.44
AN18	90	1.43	3.99	0.216	0.513022	(5)	0.512895	7.27
AN46	90	4.54	13.50	0.202	0.513020	(8)	0.512901	7.39
AN52	90	1.88	5.30	0.213	0.513021	(3)	0.512896	7.28
AN53	90	1.85	5.41	0.206	0.513020	(5)	0.512899	7.35
AN72	90	1.87	5.44	0.207	0.512999	(5)	0.512877	6.92
AN81	90	1.86	5.20	0.215	0.513020	(4)	0.512893	7.24
AN86	90	5.12	15.16	0.203	0.513012	(4)	0.512892	7.22
AN99	90	2.01	6.00	0.202	0.513008	(4)	0.512889	7.16
AN110	90	1.92	5.68	0.203	0.513020	(5)	0.512900	7.38
BN17	90	3.22	9.46	0.206	0.513027	(6)	0.512906	7.49
BN19	90	1.58	4.45	0.214	0.513025	(5)	0.512899	7.35
BN31	90	0.84	2.16	0.236	0.513044	(3)	0.512905	7.47
				Herradura				
AH5	85	2.40	7.07	0.204	0.513002	(4)	0.512888	7.02
AH8	85	1.50	4.19	0.215	0.513079	(3)	0.512960	8.41
BH11	85	1.67	4.96	0.203	0.513009	(4)	0.512896	7.17
				Tortugal				
TG4	90	1.42	6.04	0.141	0.512823	(5)	0.512740	4.24
TG8	90	3.01	11.58	0.156	0.512858	(5)	0.512766	4.75
TG9	90	4.59	21.00	0.132	0.512875	(3)	0.512798	5.37
TG13	90	2.11	6.16	0.206	0.512998	(4)	0.512877	6.91
BC17	90	2.17	6.17	0.212	0.513104	(11)	0.512979	8.92
				Golfito				
GO1	80	3.73	11.09	0.202	0.513050	(5)	0.512944	7.98
GO2	80	2.74	7.65	0.216	0.513035	(6)	0.512922	7.55
GO4	80	2.40	6.90	0.209	0.513069	(8)	0.512959	8.28
				Burica				
BUR4	80	1.76	5.10	0.208	0.513020	(11)	0.512911	7.34
BUR11	80			*0.207*	0.513031	(5)	0.512923	7.56
BUR12	80			*0.207*	0.513033	(4)	0.512925	7.60
BUR13	80	2.89	8.47	0.205	0.513032	(3)	0.512925	7.60
BUR14	80			*0.207*	0.513036	(6)	0.512928	7.66
				Quepos				
AQ8	60	5.19	18.95	0.165	0.512956	(4)	0.512891	6.45
AQ16	60	3.99	14.62	0.164	0.512945	(5)	0.512881	6.24
AQ19	60	5.47	20.00	0.165	0.512940	(5)	0.512875	6.14

Table 4. (continued)

Sample	Age, Ma	Sm, ppm	Nd, ppm	$^{147}Sm/^{144}Nd$	$^{143}Nd/^{144}Nd_m$	±2σ	$^{143}Nd/^{144}Nd_{in}$	εNdt
				Quepos				
AQ22	60	5.04	19.29	0.157	0.512936	(5)	0.512874	6.12
AQ28	60	2.29	8.44	0.164	0.512935	(4)	0.512871	6.04
AQ43	60	4.81	17.92	0.162	0.512963	(4)	0.512900	6.61
BQ32	60	2.68	7.53	0.214	0.513068	(6)	0.512984	8.26
				Osa				
OS2	60	2.80	7.92	0.213	0.513032	(4)	0.512949	7.56
OS6	60	2.03	4.58	0.267	0.513191	(4)	0.513086	10.25
OS9	60	1.66	4.75	0.210	0.513014	(5)	0.512932	7.24
OS16	60	2.44	6.69	0.219	0.513142	(4)	0.513056	9.66
				DSDP Leg14/16				
				Coiba Ridge				
155-1	20	4.07	15.69	0.156	0.513018	(8)	0.512998	7.52
				Carnegie Ridge				
157-5	5	4.42	15.12	0.176	0.513019	(6)	0.513013	7.45
				Cocos Ridge				
158-1	10	4.01	13.74	0.176	0.512961	(14)	0.512950	6.33
				Cocos Plate				
084-1	20	2.60	7.20	0.218	0.513148	(7)	0.513120	9.90

[a]Sm and Nd concentrations from ICP-MS. See Table 3 footnote.

spheric ratios, probably reflecting alteration and loss of radiogenic ^{40}Ar of some matrix fragments with higher atmospheric ^{40}Ar (Table 6). Mean apparent ages with $^{40}Ar/^{36}Ar_i$ = 295.5 weighted by the inverse variance were calculated and are quoted throughout the paper with 2σ uncertainties. The geological timescale of *Gradstein and Ogg* [1996] is used throughout the paper.

3. Geochronology: Analytical Results and General Geology

3.1. Santa Elena (Circa 124–109 Ma)

[6] The Santa Elena Peninsula consists of a south to southwest verging tectonic nappe [*Azéma and Tournon*, 1982; *Frisch et al.*, 1992] which places serpentinized peridotite above igneous and sedimentary strata (Figure 2). The footwall can be subdivided into three lithological units. Unit I contains a volcanic, sedimentary succession of vesicular, alkaline pillow lavas, massive basalts, radiolarites, radiolarite breccias, and alkaline dikes (Figure 2), which has been interpreted to represent a seamount/ocean island complex and/or a tectonic mélange [*Frisch et al.*, 1992; *Tournon*, 1994]. The radiolaria biostratigraphy of Unit I ranges from Pliensbachian to Cenomanian (196–94 Ma) [*Astorga*, 1997; *DeWever et al.*, 1985; *Schmidt-Effing*, 1980]. Owing to poor fossil preservation and the lack of primary contacts resulting from severe faulting, dating of the igneous rocks through biostratigraphic means is not possible. Unit II is made up of tholeiitic pillow lavas. An aphyric pillow basalt (SE6) from Cocinero island (Figure 2) gives a $^{40}Ar/^{39}Ar$ whole rock age of 109.0 ± 2.0 Ma (Table 6 and Figure 3). Unit III is mainly intrusive. Plagioclase from a layered gabbro complex at Playa Nancite (SE2, Figure 2) yields an $^{40}Ar/^{39}Ar$ age of 124.0 ± 4.0 Ma (Table 6 and Figure 3). The peridotitic hanging

Table 5. Pb Isotope Data From Costa Rican Igneous Basement Complexes[a]

Sample	Age, Ma	U, ppm	Th, ppm	Pb, ppm	$^{206}Pb/^{204}Pb_m$	±2σ	$^{207}Pb/^{204}Pb_m$	±2σ	$^{208}Pb/^{204}Pb_m$	±2σ	$^{206}Pb/^{204}Pb_{in}$	$^{207}Pb/^{204}Pb_{in}$	$^{208}Pb/^{204}Pb_{in}$
					Santa Elena								
SE2*	120	0.01	0.02	0.12	18.348	(3)	15.501	(3)	37.903	(8)	18.264	15.497	37.839
SE3*	120	0.03	0.05	0.30	18.278	(2)	15.481	(2)	37.773	(6)	18.169	15.476	37.709
SE6*	120	0.05	0.09	0.24	18.383	(4)	15.512	(4)	37.861	(9)	18.130	15.499	37.716
SE27*	120	0.08	0.16	0.62	18.166	(3)	15.473	(2)	37.670	(6)	18.016	15.466	37.573
SE20*	120	1.07	4.06	2.30	19.384	(2)	15.620	(2)	39.233	(6)	18.814	15.592	38.527
					Nicoya								
AN2	90	0.142	0.456	0.112	19.903	(7)	15.623	(6)	39.673	(14)	18.726	15.566	38.436
AN14	90	0.232	0.993	0.218	19.853	(3)	15.588	(3)	39.847	(7)	18.867	15.541	38.463
AN18	90	0.043	0.131	0.217	18.993	(3)	15.564	(3)	38.655	(7)	18.815	15.556	38.477
AN46	90	0.180	0.414	0.376	19.150	(5)	15.553	(4)	38.682	(9)	18.718	15.532	38.356
AN52	90	0.063	0.195	0.202	19.207	(4)	15.565	(3)	38.863	(8)	18.926	15.551	38.576
AN53	90	0.066	0.198	0.248	19.067	(5)	15.555	(4)	38.734	(10)	18.825	15.544	38.498
AN72	90	0.081	0.233	0.300	19.123	(2)	15.566	(2)	38.830	(4)	18.879	15.554	38.600
AN81	90	0.068	0.199	0.213	19.120	(2)	15.557	(2)	38.815	(5)	18.833	15.543	38.539
AN86	90	0.196	0.635	0.705	19.213	(3)	15.564	(2)	38.787	(5)	18.960	15.552	38.519
AN99	90	0.078	0.221	0.260	19.128	(2)	15.580	(2)	38.867	(5)	18.856	15.567	38.614
AN110	90	0.079	0.205	0.212	19.236	(5)	15.563	(4)	38.796	(10)	18.900	15.547	38.509
BN17	90	0.111	0.327	0.101	19.788	(2)	15.586	(3)	39.338	(9)	18.782	15.538	38.362
BN19	90	0.083	0.162	0.269	19.229	(4)	15.567	(3)	38.773	(8)	18.951	15.554	38.594
BN31	90	0.017	0.055	0.081	18.931	(5)	15.566	(4)	38.573	(10)	18.739	15.557	38.373
					Herradura								
AH5	85	0.097	0.268	0.386	18.987	(4)	15.568	(3)	38.686	(8)	18.774	15.557	38.492
AH8	85	0.124	0.371	0.588	19.035	(4)	15.551	(3)	38.651	(9)	18.855	15.542	38.475
BH11	85	0.067	0.209	0.170	19.289	(4)	15.591	(3)	38.976	(8)	18.949	15.575	38.629
					Tortugal								
TG4	90	0.132	0.453	1.188	18.714	(1)	15.607	(1)	38.526	(3)	18.614	15.602	38.413
TG8	90	0.108	0.620	2.853	18.961	(2)	15.596	(2)	38.758	(5)	18.927	15.595	38.694
TG9	90	0.580	2.401	4.504	18.893	(1)	15.572	(1)	38.732	(2)	18.777	15.566	38.574
TG13	90	0.072	0.228	0.527	18.889	(2)	15.621	(1)	38.653	(4)	18.766	15.615	38.525
BC17*	90	0.08	0.22	0.25	19.064	(3)	15.596	(2)	38.774	(5)	18.793	15.583	38.518
					Golfito								
GO1	80	0.231	0.645	0.318	19.154	(4)	15.567	(3)	38.733	(8)	18.570	15.540	38.198
GO2	80	0.089	0.321	0.204	19.116	(4)	15.569	(3)	38.740	(9)	18.765	15.552	38.325
GO4	80	0.083	0.230	0.335	18.894	(4)	15.553	(3)	38.494	(7)	18.697	15.543	38.315
					Burica								
BUR4	80	0.053	0.161	0.159	19.164	(3)	15.558	(2)	38.773	(6)	18.899	15.546	38.507
BUR11	80	0.077	0.195	0.150	19.282	(3)	15.573	(3)	38.814	(7)	18.868	15.553	38.470
BUR12	80	0.072	0.196	0.113	19.407	(6)	15.585	(5)	38.916	(13)	18.891	15.560	38.454
BUR13	80	0.085	0.246	0.115	19.419	(4)	15.572	(3)	38.949	(9)	18.819	15.544	38.381
BUR14	80	0.046	0.157	0.087	19.239	(7)	15.567	(5)	38.853	(13)	18.809	15.546	38.376
					Quepos								
AQ8	60	0.379	0.964	0.616	19.417	(2)	15.590	(2)	39.012	(5)	19.044	15.573	38.700
AQ16	60	0.261	0.737	0.585	19.438	(3)	15.596	(2)	39.081	(6)	19.168	15.583	38.830
AQ19	60	0.341	1.027	0.825	19.321	(2)	15.587	(1)	38.943	(4)	19.072	15.575	38.695

Table 5. (continued)

Sample	Age, Ma	U, ppm	Th, ppm	Pb, ppm	$^{206}Pb/^{204}Pb_m$	±2σ	$^{207}Pb/^{204}Pb_m$	±2σ	$^{208}Pb/^{204}Pb_m$	±2σ	$^{206}Pb/^{204}Pb_{in}$	$^{207}Pb/^{204}Pb_{in}$	$^{208}Pb/^{204}Pb_{in}$
							Quepos						
AQ22	60	0.387	1.198	0.600	19.519	(4)	15.599	(4)	39.191	(9)	19.126	15.580	38.792
AQ28	60	0.156	0.470	0.345	19.292	(3)	15.570	(3)	38.920	(7)	19.019	15.557	38.649
AQ43	60	0.286	0.906	0.742	19.293	(3)	15.590	(2)	38.944	(5)	19.059	15.579	38.702
BQ32	60	0.112	0.285	0.198	19.082	(18)	15.567	(15)	38.718	(37)	18.742	15.551	38.434
							Osa						
OS2	60	0.087	0.248	0.391	19.077	(4)	15.563	(3)	38.618	(8)	18.944	15.557	38.493
OS6	60	0.052	0.050	0.176	18.606	(4)	15.516	(3)	38.002	(8)	18.433	15.508	37.946
OS9	60	0.071	0.187	0.271	18.720	(3)	15.585	(2)	38.477	(6)	18.564	15.578	38.342
OS16	60	0.038	0.143	0.077	18.755	(10)	15.542	(10)	38.388	(21)	18.464	15.528	38.025
							DSDP Leg14/16						
							Coiba Ridge						
155-1	20	1.114	1.336	0.843	18.954	(1)	15.575	(1)	38.625	(3)	18.625	15.560	38.495
							Carnegie Ridge						
157-5	5	0.209	0.592	0.587	18.971	(1)	15.558	(1)	38.573	(3)	18.935	15.557	38.540
							Cocos Ridge						
158-1	10	0.332	0.764	0.662	19.343	(2)	15.603	(2)	39.006	(6)	19.293	15.601	38.968
							Cocos Plate						
084-1	20	0.061	0.075	0.426	18.517	(1)	15.541	(1)	38.073	(4)	18.482	15.539	38.059

[a]Asterisk indicates U-Th-Pb from ICP–MS; others are from thermal ionization mass spectrometry–isotope dilution. See Table 3 footnote.

wall is crosscut by doleritic dikes, some of which completely recrystallized to amphibolite in narrow shear zones (Figure 2). A K/Ar age of 88.8 ± 4.4 Ma has been obtained on the secondary hornblende [*Bellon and Tournon*, 1978]. Evidence for nappe emplacement between 94 and 71 Ma comes from the youngest (Cenomanian) radiolarites in the footwall of the thrust and Late Campanian (74–71 Ma) reef limestones growing on top of the exhumed peridotites.

3.2. Nicoya, Herradura, Tortugal, Golfito, and Burica (95–74 Ma)

[7] The Nicoya complex largely consists of aphyric pillow and massive lava flows, which are locally intruded by gabbros and plagiogranites. Dismembered radiolarite sequences of up to ~100-m thickness (Figure 2) range from Callovian to Santonian (164–84 Ma) [e.g., *Baumgartner*, 1984; *Schmidt-Effing*, 1979]. Rare occurrences of fossil-bearing intrapillow sediments, for example at Montezuma (south Nicoya), indicate Cenomanian/Touronian (94 Ma) eruption ages [*Azéma and Tournon*, 1980; *Tournon and Alvarado*, 1997]. *Sinton et al.* [1997] carried out $^{40}Ar/^{39}Ar$ step-heating analyses on seven lavas from Nicoya and obtained plateau ages between 92.5 ± 5.4 Ma and 88.0 ± 0.7 Ma. Two intrusive rocks of their study gave plateau ages of 83.8 ± 1.1 Ma and 83.2 ± 1.3 Ma. We dated a pillow lava from Playa Tambor (south Nicoya) at 94.7 ± 1.8 Ma and plagioclase from a plagiogranite from north Nicoya at 87.5 ± 1.8 Ma (Table 6 and Figure 3). Taken together the geochronological data suggest formation of the igneous basement over a relatively short time interval [*Sinton et al.*, 1997] between circa 95 and 83 Ma, which is in sharp contrast to the extensive biostratigraphic record of the radiolarites (164–84 Ma).

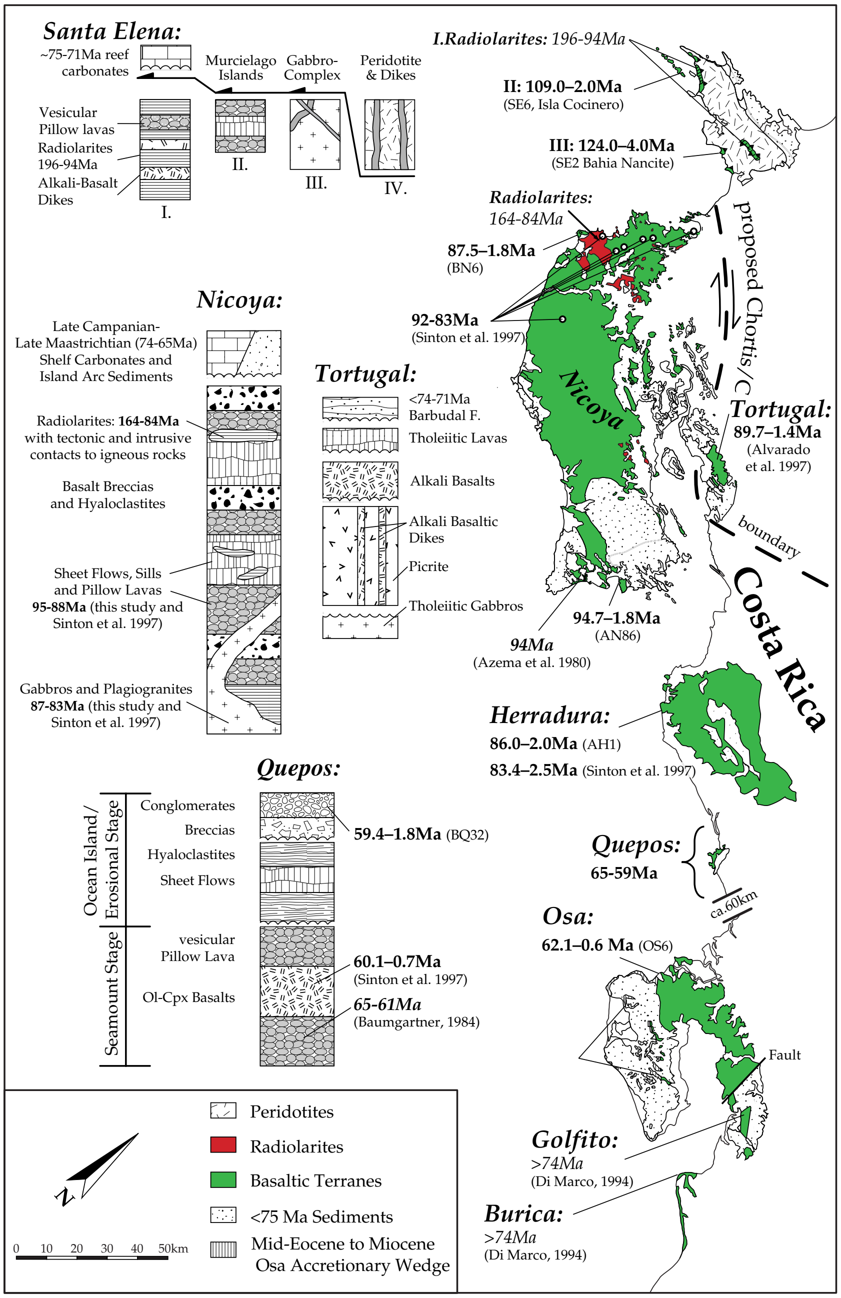

Figure 2. Basic igneous complexes along the Pacific Coast of Costa Rica after *Tournon and Alvarado* [1997] and inferred lithostratigraphic columns. Structural relations for the Santa Elena Peninsula are from *Astorga* [1997] and this study. The $^{40}Ar/^{39}Ar$ age dates (in bold type) of the igneous basement are from this study and that of *Sinton et al*. [1997]. Biostratigraphic ages of fossils from intrapillow sediments are in bold italic type. Other biostratigraphic ages (in italic type) are primarily from radiolarians and are often considerably older than the radiometric ages of the igneous rocks and intruded or in faulted contact with the igneous rocks. Proposed boundary between the Chortis and Chorotega blocks is based on geochemical (this study) and geophysical observations [*Goedde*, 1999].

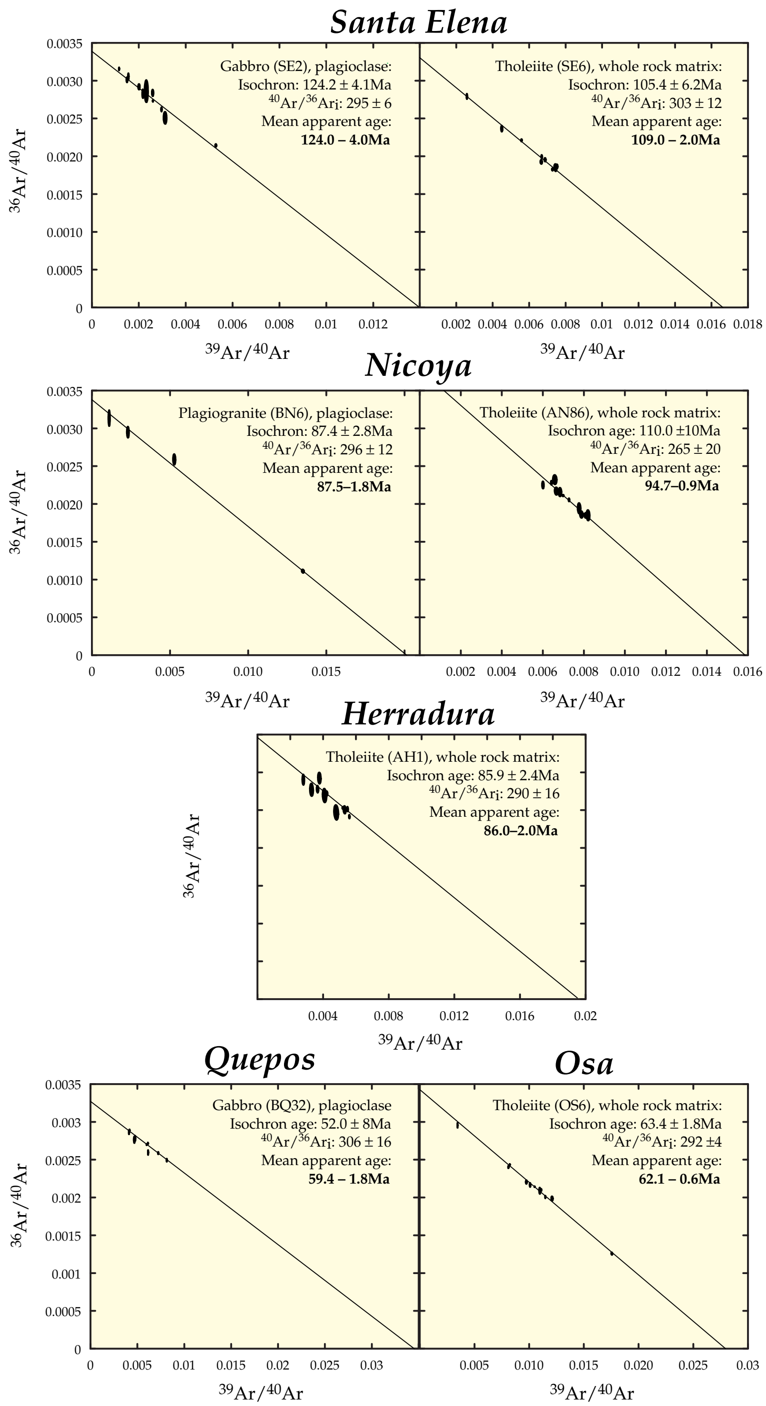

Figure 3. Argon isotope correlation diagrams of plagioclase separates and whole rock matrices from the Santa Elena, Nicoya, Herradura, Quepos, and Osa igneous complexes. Regressions and isochrons were calculated after *York* [1969]. Single-crystal and matrix analyses are shown with 1σ error ellipses. Isotope ratios are normalized to $J = 1.0 \times 10^{-3}$.

[8] The Herradura complex (Figure 2) is made up of pillow lavas and sheet flows and is thus volcanologically very similar to the Nicoya igneous complex. *Sinton et al.* [1997] dated massive tholeiitic basalt from Playa Jaco at 83.4 ± 2.5 Ma with $^{40}Ar/^{39}Ar$ incremental heating. Laser $^{40}Ar/^{39}Ar$ dating of a tholeiitic whole rock sample (Table 6 and Figure 3) from the same area yields an $^{40}Ar/^{39}Ar$ age of 86.0 ± 2.0 Ma within error of the incremental heating results. The occurrence of late Campanian through Maastrichian (74–65 Ma) radiolarites and globotruncana faunas [*Hein et al.*, 1983; *Tournon and Alvarado*, 1997] suggests that the lavas represent the lowermost stratigraphic unit in this area. The cooling ages of the Herradura lavas overlap with the crystallization ages of the Nicoya intrusions, indicating that magmatism in both areas was contemporaneous.

[9] The Tortugal igneous complex (Figure 2) consists of a picritic basal unit, intruded by alkali basaltic dikes and an upper unit consisting of tholeiitic lava and gabbro. The nature of the contact between these units is unknown [*Alvarado and Denyer*, 1998]. Discordantly overlying littoral sediments of the late Campanian (74–71 Ma) Barbudal formation [*Seyfried and Sprechmann*, 1985] provide a minimum age for the magmatic complex. Plagioclase from one of the igneous rocks yielded an $^{40}Ar/^{39}Ar$ plateau age of 89.7 ± 1.7 Ma [*Alvarado et al.*, 1997], which is within the age range reported from Nicoya and Herradura. Ultramafic and alkaline rocks, however, have not been reported from Nicoya.

[10] Golfito and Burica form the southernmost basement exposures in Costa Rica and are separated from the Osa Peninsula by a N-S trending fault (Figure 2). Late Campanian through middle Maastrichian limestones (74–68 Ma) in the Golfito area and interbedded sediments of similar age on Burica [*Di Marco*, 1994] suggest the formation of the igneous rocks before 74 Ma. We note, however, the high need for radiometric age dating in this area.

3.3. Quepos and Osa (65–59 Ma)

[11] The volcanic stratigraphy of the Quepos complex (Figure 2) provides clear evidence for the emergence of a submarine volcanic edifice above sea level and the formation of an ocean island [*Hauff et al.*, 1997]. Temporal constraints come from Danian (65–61 Ma) intrapillow sediments [*Baumgartner et al.*, 1984] and a 60.1 ± 0.7 Ma $^{40}Ar/^{39}Ar$ isochron age of a basaltic whole rock [*Sinton et al.*, 1997]. Plagioclase of a gabbroic pebble from the apron facies of the island gave an age of 59.4 ± 1.8 Ma (Table 6 and Figure 3) with the laser $^{40}Ar/^{39}Ar$ single-crystal method. Radiometric and biostratigraphic ages suggest that the seamount/ocean island volcano was active between 59 and circa 65 Ma.

[12] The Osa Peninsula to the southwest of Quepos complex (Figure 2) consists of tectonized aphyric basaltic pillow lavas and sheet flows, which are locally intruded by fine-grained gabbros. K/Ar ages of 17 basaltic whole rock samples give a mean value of 60.2 ± 7.6 Ma [*Berrangé et al.*, 1989]. A pillow basalt from western Osa (OS6, Figure 2) produced a whole rock $^{40}Ar/^{39}Ar$ age of 62.1 ± 0.8 Ma (Table 6 and Figure 3) in good agreement with the mean of the K/Ar ages.

[13] In summary, the presently available radiometric and biostratigraphic age data imply formation of the early Costa Rican basement in three distinct time intervals. The earliest magmatism is documented in tectonic slivers of the Santa Elena Peninsula (124–109 Ma), followed by an intermittent phase lasting from 95 to 74 Ma recorded in the Nicoya, Herradura, Tortugal, Golfito, and Burica igneous complexes. The younger Quepos and Osa complexes formed between 65 and 59 Ma. Although this

stratigraphic framework is still preliminary, it is nevertheless important for a meaningful interpretation of the geochemical data presented in section 4.

4. Geochemistry: Analytical Results

4.1. Santa Elena (Circa 124–109 Ma)

[14] The total SiO_2 versus alkali diagram (Figure 4) illustrates that a tholeiitic series and an alkaline lava series exist within the Santa Elena Peninsula. As will be shown below, these compositional groups formed in different tectonic-magmatic settings.

4.1.1. Rocks with island arc basalt affinities

[15] Pillow lavas (SE6) and dikes (SE3, -22a, b, -27, -31, and 33) have tholeiitic basalt to basaltic andesitic and basaltic-trachyandesitic compositions (Figure 4) and have almost identical incompatible element characteristics (Figure 5a) with a general depletion of incompatible elements (e.g., $(La/Yb)_N = 0.45 \pm 0.15$, $N = 4$). The relative depletion of Nb and Ta (e.g., $(Nb/La)_N = 0.39 \pm 0.7$) and relative enrichment of mobile elements such as U, Pb, Ba, K, and Sr over immobile elements as is reflected by low Nb/U = 6–17, Ce/Pb = 6–20 (except SE6 due to Pb loss during alteration), and high Ba/La = 24–52 and K/La = 630–2000 are characteristic of primitive subduction zone magmas such as those of the Marianas [e.g., *Elliot et al.*, 1997] (see Figure 6a). The intrusive rocks (SE2) have similar incompatible element characteristics at significantly lower element concentrations, reflecting the accumulation of the major crystal phases plagioclase and pyroxene. Initial Pb isotope ratios (Figures 10a and 10b) are relatively unradiogenic ($(^{206}Pb/^{204}Pb)_{in}$ = 18.01–18.26, $(^{207}Pb/^{204}Pb)_{in}$ = 15.46–15.49, and $(^{208}Pb/^{204}Pb)_{in}$ = 37.57–37.83) and form a linear array slightly above the Northern Hemisphere reference line (NHRL) [*Hart*, 1984]. These characteristics and radiogenic initial $(^{143}Nd/^{144}Nd)_{in} = 0.51298 \pm 1$ ($\varepsilon Nd_i = 9.6 \pm 0.21$) as well as $(Sm/Nd)_N > 1$ indicate a derivation from a long-term depleted mantle source that overlaps the field of Pacific mid-ocean ridge basalt (MORB). Initial $^{87}Sr/^{86}Sr$ ratios are relatively unradiogenic (0.7029–0.7031) but can reach 0.7047 in the gabbros (Figure 9).

[16] The increasing $(^{87}Sr/^{86}Sr)_{in}$ from 0.7029 in the leached pillow basalt to 0.7047 in the leached gabbro sample despite similar Nd and Pb isotopic composition could result either from (1) assimilation of altered oceanic crust or (2) contamination by fluids dehydrated from a seawater-altered subducting slab. In conclusion, the isotope and trace element characteristics of the tholeiitic basalts, basaltic andesites, and basaltic trachy-andesites on Santa Elena are consistent with their generation in a subduction zone environment.

4.1.2. Rocks with ocean island basalt affinities

[17] Dikes and vesicular pillow lavas in Unit I have tephritic, trachy-basaltic, and phono-tephritic compositions (Figure 4). Incompatible elements are strongly enriched relative to the more compatible elements (e.g., $(La/Yb)_N = 15.9$ and $(Nb/La)_N = 1.2$), whereas Pb is markedly depleted (Figure 5b). These characteristics are similar to modern ocean island basalts (OIBs). Unradiogenic $(^{143}Nd/^{144}Nd)_{in} = 0.51264$ ($\varepsilon Nd_i = 3.0$) and radiogenic $(^{87}Sr/^{86}Sr)_{in} = 0.7035$ indicate derivation from a long-term enriched mantle source (Figure 9), while initial Pb isotope ratios (e.g., $(^{206}Pb/^{204}Pb)_{in} = 18.81$) have intermittent compositions (Figures 10a and 10b).

4.2. Nicoya, Herradura, Golfito, Burica, and Tortugal (Circa 95–74 Ma)

[18] Volcanism from 95 to 74 Ma is dominated by tholeiitic to basaltic andesitic lavas (SiO_2 = 49–53 wt % and MgO = 3–11 wt %, Table 1).

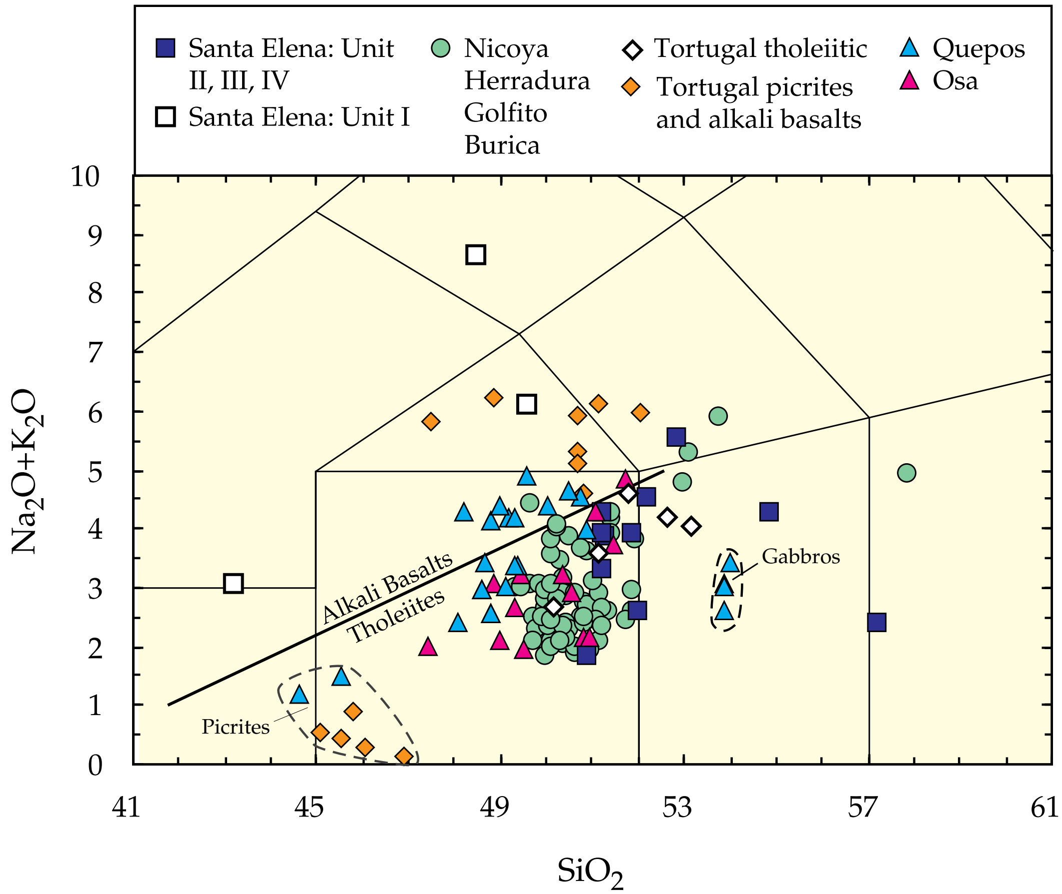

Figure 4. Chemical classification of igneous rocks from Costa Rican igneous complexes on the total alkali versus SiO_2 diagram after *Le Maitre* [1989]. Alkaline-subalkaline division line after *Macdonald and Katsura* [1964]. The majority of samples have tholeiitic composition; however, lavas and dikes from Tortugal and Unit I of the Santa Elena Peninsula have trachytic, basaltic-trachyandesitic, tephritic, and phonotephritic compositions. Most volcanic rocks from Quepos are transitional tholeiites.

In this age group, alkali basaltic to trachybasaltic dikes and picrites enriched in incompatible elements occur only at Tortugal. The tholeiites show good correlations between MgO and immobile elements, reflecting crystal fractionation of olivine + plagioclase (plag) ± Cr-spinel [*Hauff et al.*, 1997]. Incompatible element patterns (Figures 6b, 6c, and 7a) are generally flat with relative depletions of Th, U, Pb, and P and slight enrichments in Nb and Ta (e.g., $(Nb/Th)_N = 1.93 \pm 0.37$, $N = 38$). Initial Nd isotope ratios from Nicoya and Herradura are uniform with $(^{143}Nd/^{144}Nd)_{in} = 0.51291 \pm 2$ (N = 26), while samples from Golfito and Burica show a slightly larger spread ($(^{143}Nd/^{144}Nd)_{in}$ = 0.51292 ± 7, N = 6 out of 7). Initial $^{87}Sr/^{86}Sr$ ratios of most unleached samples lie between 0.7030 and 0.7040, but some are as high as 0.7062. Severe acid leaching in hot aqua regia on a subset of samples did not always lower $^{87}Sr/^{86}Sr$ significantly (Tables 3–5). Either acid leaching may not always remove the effects of seawater alteration or the variable $(^{87}Sr/^{86}Sr)_{in}$ at constant $(^{143}Nd/^{144}Nd)_{in}$ (Figure 9) could reflect assimilation of hydrothermally altered oceanic crust or the presence of such material in the source [*Hauff et al.*, 2000]. Despite the large range in measured Pb isotope ratios (($^{206}Pb/^{204}Pb)_m$ = 18.93–19.90, $(^{207}Pb/^{204}Pb)_m$ = 15.55–15.62, $(^{208}Pb/^{204}Pb)_m$ = 38.57–39.84), initial Pb isotope ratios tightly cluster with $(^{206}Pb/^{204}Pb)_{in}$ = 18.72–18.96, $(^{207}Pb/^{204}Pb)_{in}$ = 15.53–15.57, and $(^{208}Pb/^{204}Pb)_{in}$ = 38.37–38.61 (Tables 3–5 and Figures 10a and 10b). The uniform incompatible element and initial Nd and Pb isotope signatures of the tholeiitic rocks indicate derivation from a common source. The slight positive anomaly for Nb and Ta and extreme Pb depletion provide clear evidence that they were not generated in an arc setting. On the other hand, less radiogenic Nd and more radiogenic Sr-Pb isotopic compositions compared to Pacific NMORB of similar age (Figures 9 and 10) are inconsistent with derivation from depleted upper mantle, the common source of MORB. The chemical characteristics are, however, similar to mid-Cretaceous oceanic plateaus in the western Pacific such as the Ontong Java (Figures 6b, 6c, and 7a) [*Mahoney et al.*, 1993; *Neal et al.*, 1997] and in particular to other circum-Caribbean igneous complexes of similar age, often referred to as the Caribbean Large Igneous Province (CLIP) [*Hauff et al.*, 2000; *Kerr et al.*, 1997].

[19] The picrites and alkaline rocks at Tortugal have steeply inclined incompatible element patterns (Figure 5b, e.g., $(La/Yb)_N$ = 3.8–9.5) with a depletion of highly incompatible elements such as U and Th relative to Nb and Ta, similar to modern OIB. The picrites have the lowest incompatible element concentrations but incompatible element ratios very similar to the alkali basalt dikes, consistent with formation of the picrites through olivine accumulation. Similar initial Nd (($^{143}Nd/^{144}Nd)_{in}$ = 0.51272 ± 7, εNd_i = 4.2 ± 1.0, N = 4) and Pb isotope compositions (e.g., $(^{206}Pb/^{204}Pb)_{in}$ =18.96 ± 0.17, Tables 3–5 and Figures 10a–10c) further point to a genetic relationship between these rock types. Elevated $(^{207}Pb/^{204}Pb)_{in}$ = 15.57–15.60 ($\Delta 7/4$ = 4.0–9.3) could possibly reflect subducted sediment in the source or crustal assimilation. Tholeiitic basalts (BC17) and tholeiitic gabbros (TG13) at Tortugal have flat incompatible element patterns $(La/Yb)_N$ = 0.81–0.99, radiogenic $(^{143}Nd/^{144}Nd)_{in}$ = 0.51288–0.51298 and unradiogenic $(^{206}Pb/^{204}Pb)_{in}$ = 18.74–18.79), similar to the Nicoya, Herradura, Golfito, and Burica tholeiites. The unradiogenic Nd isotope composition of the alkaline rocks and picrites precludes that they originate from the same source as that of the tholeiitic rocks. We, however, note the similarity between the incompatible element patterns and radiogenic isotope compositions of the Tortugal picrites and alkaline rocks and those of the alkaline rocks from Santa Elena (Figures 5b, 9, and 10).

4.3. *Quepos and Osa (65–59 Ma)*

[20] Within this age group, a transitional tholeiitic series (Quepos) can be distinguished from a tholeiitic series (Osa). At Quepos, covariations of CaO, Al_2O_3, and trace elements (Cr, Ni, Sr, and Ba) with MgO suggest fractionation of olivine (Ol) + clinopyroxene (Cpx) ± Cr-spinel at pressures >5 kbars, consistent with the observed phenocryst assemblage of the lavas [*Hauff et al.*, 1997]. Inclined incompatible element patterns (Figure 7b, $(La/Yb)_N$ = 3.37 ± 0.37, N = 10) and enrichment of Nb and Ta relative to the other highly incompatible elements (e.g., $(Nb/La)_N$ = 1.20 ± 0.11, N = 18) and depletion of Pb relative to other incompatible elements are characteristic of OIB. Two Quepos gabbros (BQ32 and BQ72) are slightly depleted in light REE (LREE) ($(La/Yb)_N$ = 0.77–0.83, Figure 7c). The Quepos lavas have similar initial $(^{143}Nd/^{144}Nd)_{in}$ = 0.51288 ± 1 and slightly more radiogenic $(^{206}Pb/^{204}Pb)_{in}$ = 19.08 ± 0.05 (n = 7) (Tables 3–5 and Figure 10c) than the 95–75 Ma

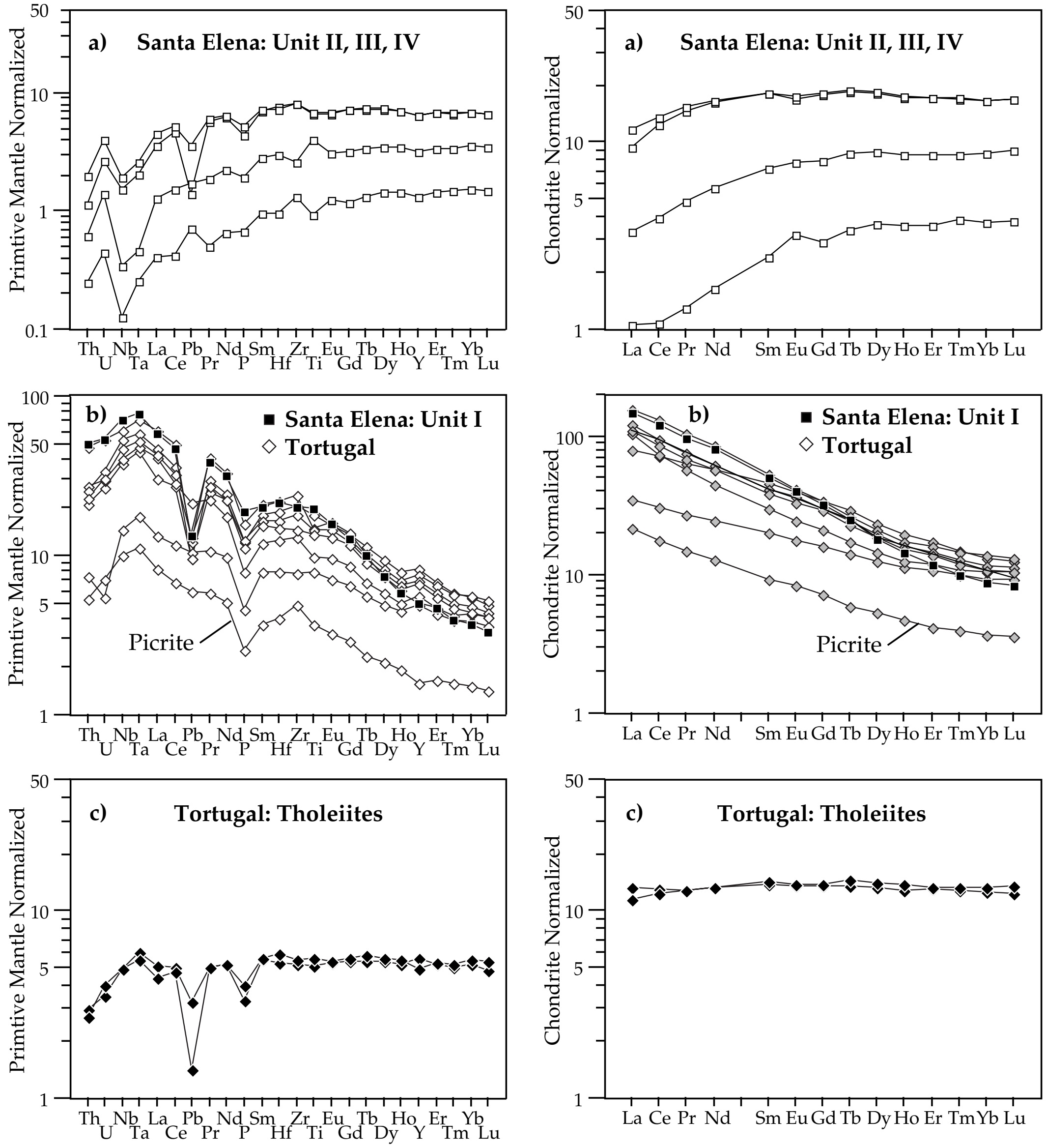

Figure 5. Incompatible element diagrams of the more immobile elements normalized to primitive mantle after *Hofmann* [1988] and rare earth elements (REE) patterns normalized to C1 chondrite after *Sun and McDonough* [1989]. Elements in both types of diagrams are arranged with increasing compatibility from left to right. (a) Tholeiites from Units II, III, and IV from the Santa Elena complex are similar to arc lavas from the Marianas [*Elliot et al*., 1997]. (b) Alkali basalts from Santa Elena Unit I and from Tortugal have nearly identical incompatible element patterns which are similar to ocean island basalts (OIB) [*Chaffey et al*., 1989; *Thirlwall*, 1997] (see Figure 6a for comparison). (c) Tholeiitic lavas and gabbros from Tortugal have patterns similar to those from Nicoya, Herradura, Golfito, and Burica. See Figure 5b for comparison.

tholeiitic complexes, indicating derivation from a similar mantle plume source. The higher incompatible element concentrations of the Quepos transitional tholeiites could reflect low-

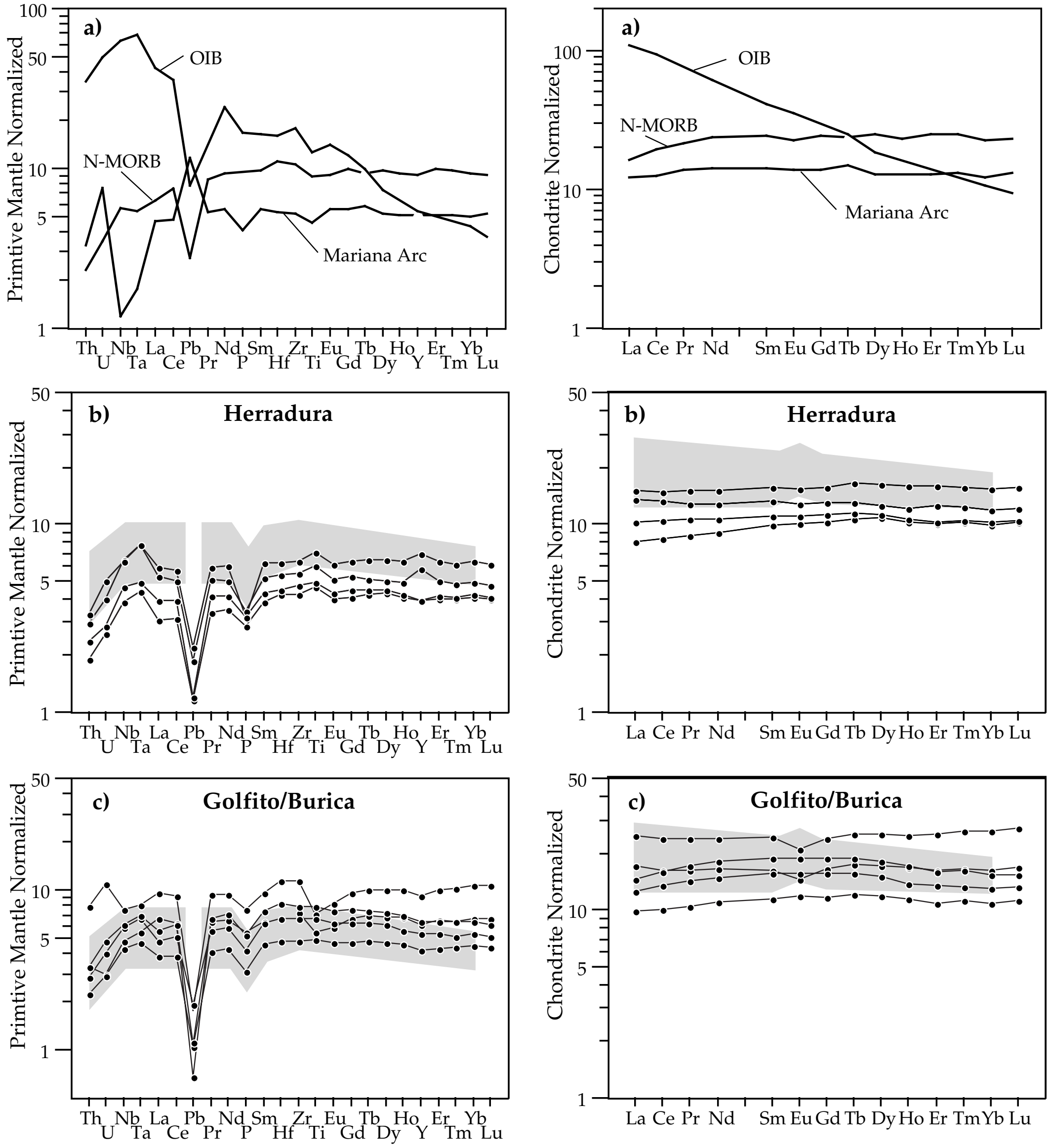

Figure 6. (a) Reference patterns for normal mid-ocean ridge basalt (NMORB) after *Hofmann* [1988], OIB after *Chaffey et al*. [1989] and *Thirlwall* [1997], and island arc basalts after *Elliot et al*. [1997]. (b) Tholeiitic lavas and gabbros from Nicoya. (c) Tholeiitic lavas and gabbros from Herradura.

er degrees of melting as suggested by greater average depths (~50 km) of melting and lower melting temperatures (~1300°C) than those estimated for the Nicoya tholeiites [see *Hauff et al*., 1997]. Although the Quepos lavas have OIB-type incompatible element patterns similar to those from Santa Elena and Tortugal, different Nd and Pb isotopic compositions exclude that the Quepos lavas were derived from the same source as that of these older OIB-type lavas.

[21] Tholeiitic lavas of the Osa Peninsula generally have flat incompatible element patterns $(La/Yb)_N$ = 0.95, except for samples

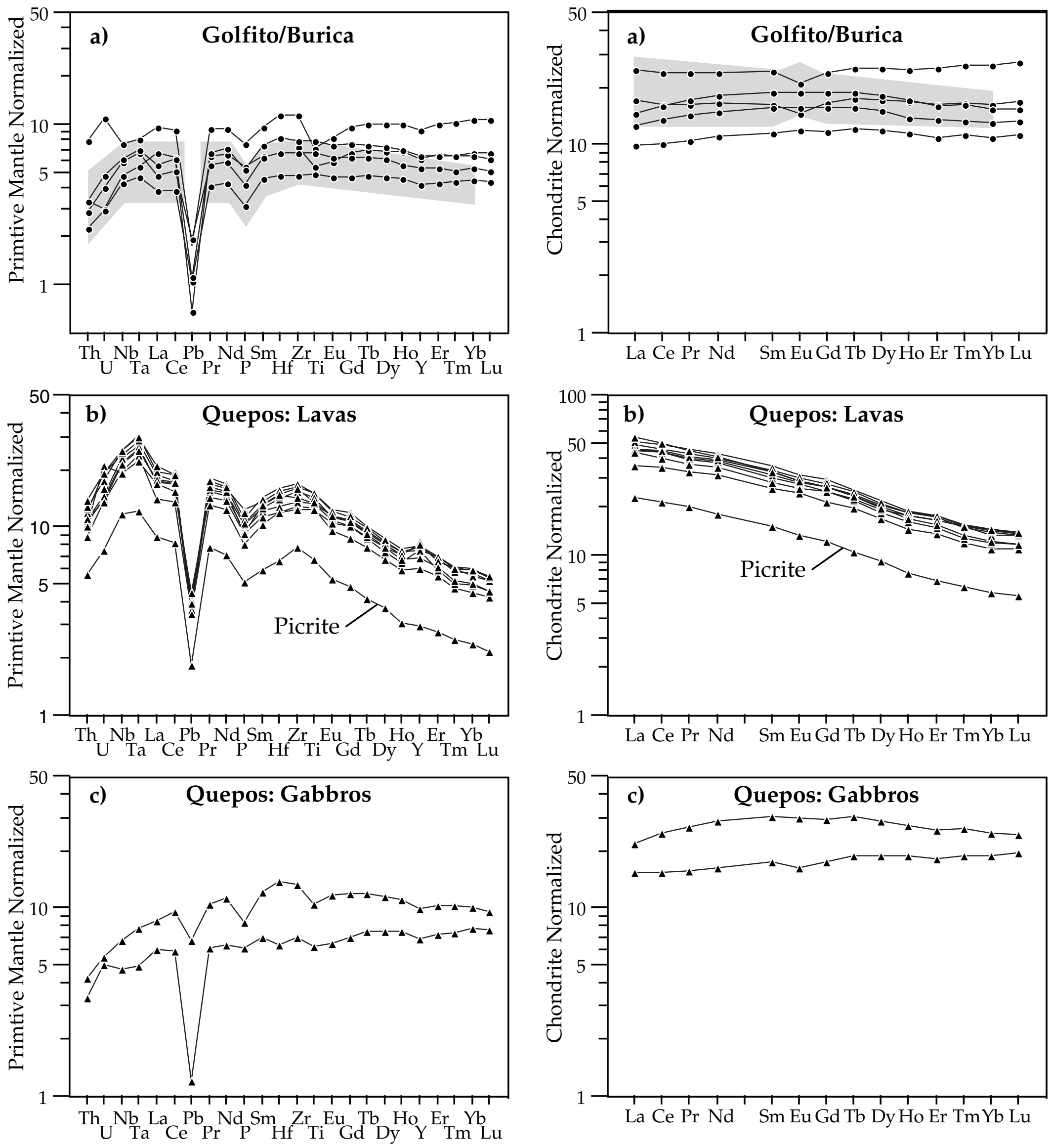

Figure 7. (a) Tholeiitic lavas and gabbros from Golfito and Burica. The latter are similar to those of the 125–90 Ma Ontong Java Plateau (shaded field after *Mahoney et al*. [1993] and *Neal et al*. [1997]). (Note no Pb and Lu concentration data are available for the Ontong Java Plateau.) (b) Incompatible element patterns of the Quepos transitional tholeiites are similar to OIB but are less enriched in incompatible elements than the Tortugal and Santa Elena alkali basalts are. (c) Quepos tholeiitic gabbros are more depleted in incompatible element patterns than the Quepos lavas are.

OS6 and OS16, which show depleted patterns with $(La/Yb)_N$ = 0.26–0.64 (Figure 8a). The Osa lavas tend toward more radiogenic Nd $((^{143}Nd/^{144}Nd)_{in}$ = 0.51293–0.51309) and less radiogenic initial Pb isotope compositions $((^{206}Pb/^{204}Pb)_{in}$ = 18.43–18.94) than the Quepos rocks, consistent with the more depleted trace element characteristics of these lavas

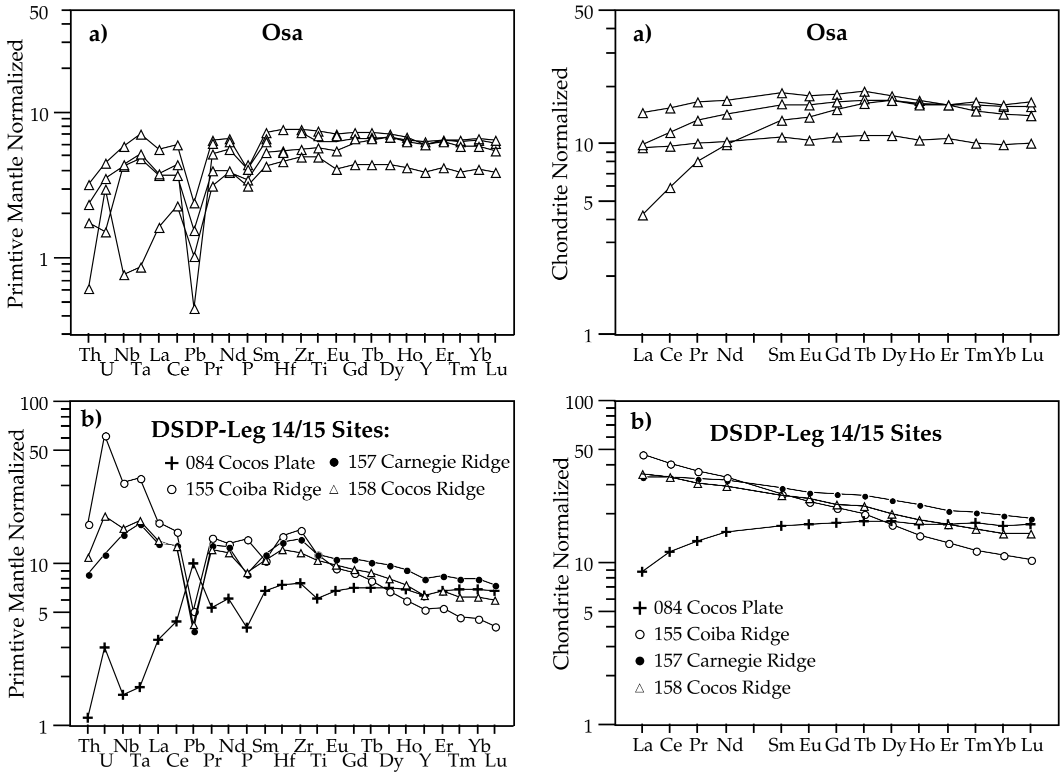

Figure 8. (a) Most Osa lavas have trace element characteristics similar to those of the Nicoya, Herradura, Golfito, and Burica lavas, except for sample OS6, which is strongly depleted in the most incompatible elements. The strong U enrichment in this sample most likely results from cold seawater alteration. (b) Incompatible element patterns of the Carnegie, Cocos, and Coiba aseismic ridges and the Cocos plate. Note the similarity of the Cocos plate basalt and the Osa pillow lava (OS6). NMORB, normal mid-ocean ridge basalt.

(Tables 3–5 and Figure 10c). Tholeiitic samples of Deep Sea Drilling Project (DSDP) Leg 14 from the Cocos and Carnegie aseismic ridges, forming part of the Miocene Galápagos hotspot track (Figure 1), have incompatible element and initial Pb and Nd isotopic ratios (Figures 10a–10c) similar to Osa, suggesting a common origin.

5. Discussion

5.1. Disputed Origin and Complex Structure of the Caribbean Basement

[22] On the basis of seismic and geochronological studies [e.g., *Maufrett and Leroy*, 1997; *Driscoll and Diebold*, 1998; *Sinton et al.*, 1998, and references therein], the existence of an oceanic flood basalt province within the Caribbean plate is now widely accepted. Yet considerable debate exists as to whether it formed in the Pacific realm or in between the Americas. Most plate tectonic reconstructions locate this part of the eastern Pacific over the Galápagos hotspot at 100–90 Ma [*Duncan and Hargraves*, 1984; *Pindell and Barrett*, 1990], whereas extrapolation of present-day, westward directed absolute plate motions of North America, South America, and the Caribbean yields an inter- or near-American position, distant from the Galápagos hotspot [*Meschede and Frisch*, 1998].

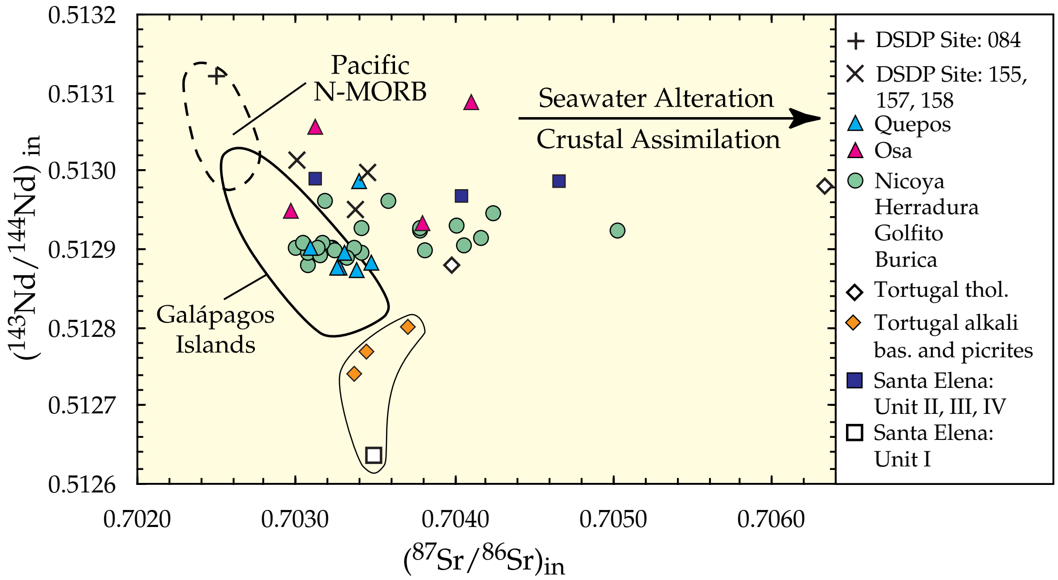

Figure 9. Initial Sr-Nd isotope correlation diagrams of Costa Rican basement complexes. Fields of the Galápagos Islands and Pacific NMORB after *White et al.* [1993] and *Janney and Castillo* [1997], respectively. Data are from Tables 3–5. Note that unleached Sr data are plotted when leached Sr data are not available.

Recent seismic studies in the eastern Caribbean sea [*Driscoll and Diebold*, 1998] and petrological studies of igneous complexes in Cuba [*Kerr et al.*, 1999] add even more complexity, because they suggest the existence of an older, pre-Cenomanian (>99 Ma), oceanic plateau within the Caribbean plate. Interestingly, multiple magmatic events are also recognized for the Ontong Java and Kerguelen oceanic plateaus [*Neal et al.*, 1997; *Storey et al.*, 1996] and underline the strong need for reliable age dating in order to more fully understand the formation of these structures. For several reasons it is at present also an open question whether the Caribbean flood basalt event is indeed related to the initiation of the Galápagos hotspot. First, the present Galápagos Islands are derived from a plume consisting of at least four distinct mantle domains [*White et al.*, 1993]. Consequently, a unique chemical fingerprint is difficult to constrain. Second, the oldest parts of the Galápagos hotspot track presently being subducted off the coast of Central and South America are 20–25 Ma [*Werner et al.*, 1999], thus leaving a temporal gap of at least 50 myr to the CLIP lavas. Through integration of geochronological and geochemical data of the Costa Rican igneous complexes of this study, we are, however, able to develop a consistent model in which the Galápagos hotspot system appears to play a major role in the evolution of the Caribbean plate and the Central American plate margin.

5.2. *Origin of the West Costa Rican Igneous Complexes*

5.2.1. Santa Elena (124–109 Ma): Part of the Chortis subduction zone

[23] The oldest radiometrically dated rocks of Costa Rica occur on the Santa Elena Peninsula (125–109 Ma). The tholeiitic to basaltic-

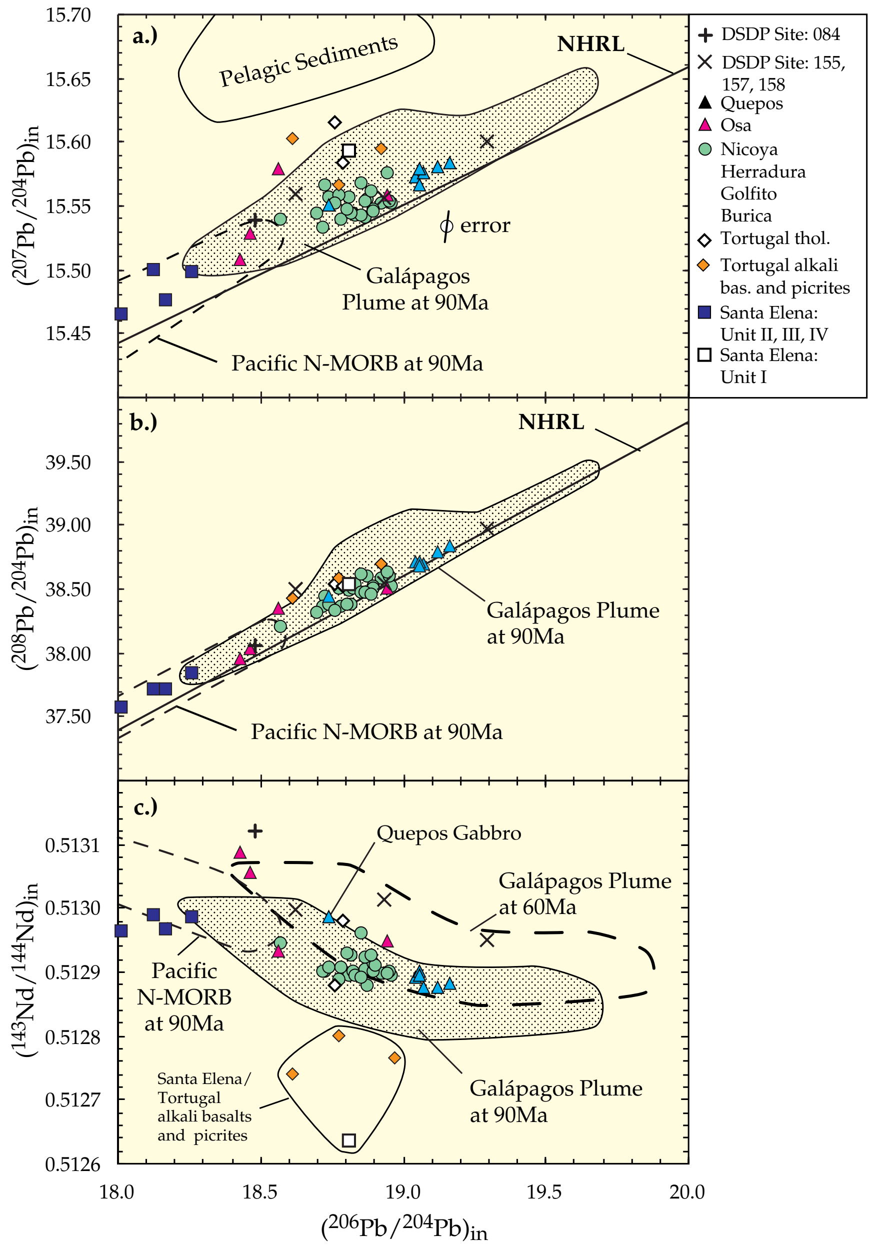

Figure 10. Initial Pb-Pb and Pb-Nd isotope correlation diagrams for Costa Rican basement complexes. All data, except island arc basalts of the Santa Elena complex, lie within the field of the Galápagos Islands [*White et al.*, 1993]. Owing to a lack of U, Th, and Pb concentration data for the Galápagos data, we assume a linear increase of μ with $^{206}Pb/^{204}Pb$ ($\mu = 10 \times {}^{206}Pb/^{204}Pb - 175$) and $^{232}Th/^{238}U = 3$ in calculating the field for the Galápagos source [*Hauff et al.*, 2000]. Northern Hemisphere reference line (NHRL) is after *Hart* [1984].

trachyandesitic rocks from Units II, III, and IV have element and isotope characteristics consistent with formation in a subduction zone environment, features so far not confirmed in any other basement complex along the Pacific Coast of Costa Rica. In contrast, the alkaline rocks from Unit I have OIB-type geochemical characteristics. In accordance with earlier suggestions by *Frisch et al.* [1992], the alkaline rocks could represent an accreted section of a geochemically enriched off-axis Pacific seamount, trapped within a

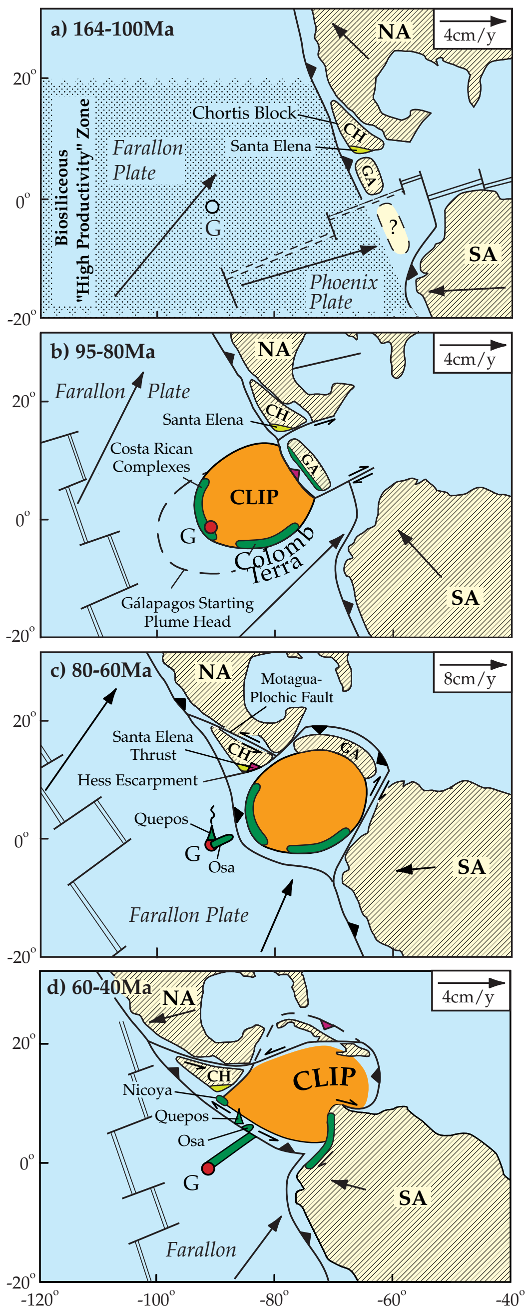

Figure 11. Geodynamic evolution of Central America based on the age and geochemistry of igneous complexes in western Costa Rica (this study) and plate tectonic reconstructions of *Duncan and Hargraves* [1984] and *Pindell and Barrett* [1990]. (a) During the Late Jurassic to mid-Cretaceous was the opening of the proto-Caribbean Sea with the Greater Antilles Arc (GA) and the Chortis block (CH at its western margin). Radiolarites are deposited in an equatorial upwelling zone of the eastern Pacific. G, the later location of the Galápagos hotspot; NA, North America; SA, South America. (b) During the mid- to Late Cretaceous was the formation of the Caribbean Large Igneous Province (CLIP) at ∼90 Ma (dashed circle) above the Galápagos hotspot. Northeastward migration of the oceanic plateau lead to collision with the Greater Antilles Arc at ∼80 Ma and caused a reversal of subduction polarity and transform faulting between the CLIP and the Chortis block and South America, respectively. (c) During the Late Cretaceous to early Tertiary, insertion of the CLIP between the Americas continued and subduction of normal oceanic crust along the western margin of the CLIP began, establishing the precursor of the present Central America Arc. Left-lateral displacement along the Motagua Polochic fault may have caused collision with the CLIP (Chorotega block) along the Hess Escarpment and thrusting of the Santa Elena complex. Above the Galápagos plume the Quepos ocean island and Osa aseismic ridges formed and were subsequently transported toward the Central American Arc. (d) During the early to late Tertiary, by late mid-Eocene (∼45 Ma) the Osa aseismic ridge and the drowned Quepos ocean island enter the Central American trench and were accreted to the CLIP crust. A widely distributed early to late Oligocene (34–28 Ma) regional unconformity throughout Central America might be related to the collision with Quepos and Osa hotspot structures that caused large-scale deformation and uplift of the entire arc as well as trench-parallel displacement of igneous basement complexes (e.g., Nicoya).

Table 6. Laser-$^{40}Ar/^{39}Ar$-Single Crystal- and Matrix Age Determinations of Costa Rican Igneous Basement Complexes

Sample	Rock Type	Material	Mass, mg min-max	Isochron Age, Ma	±2σ	$^{40}Ar/^{36}Ar$ Intercept	±2σ	MSWD	*N*	Apparent Age, Ma	±2σ
				Santa Elena							
SE2	gabbro	plagioclase	0.13–0.56	124.2	±4.1	295	±6	2.78	11	124.0	±4.0
SE6	tholeiite	w.r. matrix		105.4	±6.2	303	±12	2.14	9	109.0	±2.0
				Nicoya							
AN86	tholeiite	w.r. matrix	0.10–1.20	110.0	±10.0	265	±20	1.08	11	94.7	±1.8
BN6	P-granite	plagioclase	0.14–0.36	87.4	±2.8	296	±12	1.21	4	87.5	±1.8
				Herradura							
AH1	tholeiite	w.r. matrix	0.10–1.20	85.9	±2.4	290	±16	1.36	11	86.0	±2.0
				Quepos							
BQ32	gabbro	plagioclase	0.14–0.48	52.0	±8.0	306	±10	2.63	9	59.4	±1.8
				Osa							
OS6	tholeiite	w.r. matrix	0.12–1.09	63.4	±1.8	292	±4	2.23	11	62.1	±0.6

subduction zone sometime between the Cenomanian (99–94 Ma, age of the youngest radiolarites) and the Maastrichtian (71–65 Ma, exhumation of the peridotites). It is interesting to note that serpentinized peridotites also occur along the San Juan River and in the Tonjibe borehole (see Figure 1 of this work and *Astorga* [1992] for additional information). The east-west alignment of the peridotites seems to reflect a suture zone [*Tournon et al.*, 1995] that coincides with the Hess Escarpment, a structural boundary between the oceanic crust of the Chorotega block and the continental crust of the Chortis block [*Meschede and Frisch*, 1998, and references therein]. The Chortis block is a segment of the North American craton (Figure 11) that migrated eastward along the left-lateral Motagua-Polochic fault zone on its northern boundary from Campanian to Oligocene times (84–34 Ma) into its present position (see Figure 11b) [*Meschede and Frisch*, 1998, and references therein]. We interpret the Santa Elena complex as an uplifted mantle wedge of the Chortis subduction zone, originally located in front of Mexico (Figure 11a). This view is also supported by the strong serpentinization, which indicates the presence of abundant fluids that were possibly derived from the dehydrating subducting slab. The depleted Sr-Nd-Pb isotopic signatures of the melts suggest that the mantle wedge resembled Pacific NMORB mantle. Up to 90° counterclockwise rotations of paleomagnetic declination vectors within the Santa Elena thrust point to a south to southwest directed primary movement along the fault [*Frisch et al.*, 1992]. Moreover, these block rotations can only be explained with a left-lateral transform component that translates into an eastward migration of the Chorotega block relative to the Chortis block (Figure 11b). The late Campanian exhumation of the peridotites coincides with the onset of displacement along the Motagua-Polochic fault [*Meschede and Frisch*, 1998, and references therein]. Late Campanian coral reefs developed on top of the peridotite massifs and provide excellent temporal constraints for the collision of the Chortis block with the Chorotega block at 75–71 Ma.

Table A1. Sample Locations of Costa Rican Igneous Complexes Based on 1:50,000 Topographic Maps of the Instituto Geografico de Costa Rica

			Map Coordinates	
Sample	Locality	Map	Longitude	Latitude
		Santa Elena		
SE2	Bahia Nancite	Ahogados	346.50	311.00
SE3	Bahia Nancite	Ahogados	346.50	311.00
SE6	Isla Cocinero	Santa Elena	327.50	315.60
SE18	NW Punta Respinque	Santa Elena	331.50	317.50
SE20	NW Punta Respinque	Santa Elena	330.50	318.40
SE21	NW Punta Respinque	Santa Elena	330.50	318.40
SE22a,b	Playa Gringo	Santa Elena	328.90	321.80
SE24	Playa Gringo	Santa Elena	328.90	321.80
SE27	Playa Gringo	Santa Elena	328.30	321.50
SE30	Playa Morro	Santa Elena	327.90	321.40
SE31	Playa Morro	Santa Elena	327.90	321.40
SE33	Playa Morro	Santa Elena	327.90	321.40
SE34	Isla Cocinero	Santa Elena	346.50	311.00
		Nicoya		
AN2	Playa Potrero	Matapalo	341.45	271.30
AN3	Playa del Coco	Carillo Norte	349.00	282.15
AN14	Punta Cirial	Carillo Norte	347.40	281.45
AN18	NE Isla Loros	Matapalo/Punta Gorda	340.10	267.45
AN21	Lagarto	Marbella	339.75	232.6
AN23	Lagarto	Marbella	339.55	233.10
AN24	Junquillal Playa Blanca	Villarreal	337.05	240.05
AN28	Punta Concava	Cerro Azul	373.40	205.30
AN36	Puerto Carillo	Cerro Brujo	345.55	224.05
AN46	Puerto Carillo	Cerro Azul	373.40	205.30
AN52	Punta Islita	Cerro Azul	382.45	203.70
AN53	Peña Guastomate	Cerro Azul	386.75	202.85
AN54	Peña Guastomate	Cerro Azul	386.75	202.10
AN56	2.65km South Belen	Cerro Brujo	371.60	221.10
AN63	NE Punta Coyote	Puerto Coyote	396.80	194.20
AN64	NE Punta Coyote	Puerto Coyote	397.10	194.75
AN71	2km SSW Montezuma	Cabuya	418.50	180.10
AN72	1.6km SSW Montezuma	Cabuya	418.60	180.75
AN75	0.8km SSW Montezuma	Cabuya	418.75	181.45
AN76	North Rocca los Almendros	Cabuya	420.40	183.35
AN81	0.3km NW Piedra Amarilla	Rio Ario	426.85	188.35
AN86	1.4km West Tambor	Rio Ario	426.45	188.75
AN87	quarry Tambor-Cobano	Rio Ario	427.85	188.55
AN99	Pochote Queb el Coco	Tambor	429.20	191.30
AN102	Playa los muertos	Tambor	427.45	192.20
AN108	Acoyapa	Matambu	396.35	229.70
AN110	Mountain pass near Huacas	Matapalo/Punta Gorda	343.85	261.00
AN119	Quarry Playas del Coco-Sardinal	Carillo Norte	353.45	280.15
AN121	Playas del Coco	Carillo Norte	349.25	281.90
AN123	Punta Monte del Barco	Carillo Norte	356.70	288.45
AN124	East of Punta Conchal	Matapalo/Punta Gorda	339.60	265.35
AN125	East of Punta Conchal	Matapalo/Punta Gorda	339.95	265.25
AN126	Punta Gorda above Playita Manzanillo	Matapalo/Punta Gorda	341.50	279.40

Table A1. (continued)

Sample	Locality	Map	Map Coordinates	
			Longitude	Latitude
		Nicoya		
AN127	Road Playa de el Coco-Playa Ocotal	Matapalo/Punta Gorda	348.30	281.10
AN128	Road Playa de el Coco-Playa Ocotal	Matapalo/Punta Gorda	348.30	281.10
BN14	North Playa Brasilito	Matapalo	340.20	367.65
BN16	Potrero	Matapalo	341.90	271.30
BN17	Playa Guacamaya	Punta Gorda	339.55	278.00
BN19	Road Sardinal-Nuevo Colon-Potrero	Carillo Norte	349.55	276.35
BN20	West of Playa Matapalo	Punta Gorda	344.30	279.45
BN21	Nuevo Colon-Zapotal	Carillo Norte	345.00	274.15
BN22	3km East Potrero	Belen	345.10	272.00
BN23	Ocotal	Carillo Norte	347.40	281.20
BN26	South of Playa Hermosa	Carillo Norte	351.85	283.85
BN29	Punta Arenilla	Carillo Norte	355.85	286.85
BN30	Road Playa del Coco-Sardinal	Carillo Norte	355.15	278.85
BN31	Cerro Brasilar	Carillo Norte	341.90	269.50
BN33	Montezuma	Cabuya	419.85	182.20
		Herradura		
AH1	road cuts SE of Jaco	Herradura	394.65	393.65
AH2	road cuts SE of Jaco	Herradura	394.65	393.65
AH4	road cuts SE of Jaco	Herradura	395.05	393.15
AH5	Playa Jaco	Herradura	392.45	397.10
AH6	Playa Jaco	Herradura	394.55	393.85
AH8	Playa Herradura	Herradura	389.95	400.35
BH11	road cuts SE of Jaco	Herradura	395.10	393.50
		Tortugal		
TG1	Higuerillas	Abangares	422.30	240.70
TG2	Higuerillas	Abangares	422.50	240.40
TG5	Queb Barbudal	Abangares	416.80	242.60
TG3	NNE Fina Carrizal	Abangares	426.03	238.65
TG4	Quarry Publo Nuevo	Abangares	414.50	246.00
TG6	South Cerro Delirio	Abangares	418.70	242.70
TG7	South Cerro Delirio	Abangares	417.45	242.15
TG8	North Cerro Cardenales	Abangares	423.25	240.30
TG9	West of Finca San Martin	Abangares	426.15	239.80
TG10	South Cero San Cristobal	Abangares	423.50	242.70
TG11	Queb Barbudal	Abangares	416.85	243.65
TG12	Queb Barbudal	Abangares	416.85	243.65
TG13	Tortugal	Juntas	427.30	239.40
TG14	Tortugal	Juntas	427.30	239.40
TG15	South Cerro Delirio	Abangares	419.20	242.75
BC16	Tortugal	Juntas	427.50	239.60
BC17	Cerro Barbudal	Abangares	415.10	243.65
BC18	Cerro Barbudal	Abangares	415.30	243.60
		Golfito		
GO1	South Playa Cacao	Golfito	532.20	286.40
GO2	South Playa Cacao	Golfito	532.40	286.60
GO3	South Playa Cacao	Golfito	532.60	286.70

Table A1. (continued)

Sample	Locality	Map	Map Coordinates	
			Longitude	Latitude
		Golfito		
GO4	Golfito	Golfito	560.50	284.25
GO5	Golfito	Golfito	560.50	284.25
		Burica		
BUR4	mouth of Rio Claro	Pavon	558.00	261.15
BUR5	mouth of Rio Claro	Pavon	558.00	261.15
BUR11	Roca el Barco	Puerto Armuelles	577.35	241.50
BUR12	Punta la Peña	Puerto Armuelles	577.60	241.75
BUR13	Punta la Peña	Puerto Armuelles	577.60	241.75
BUR14	Punta la Peña	Puerto Armuelles	577.60	241.75
		Quepos		
AQ8	Playa Espadilla West section	Quepos	444.50	371.93
AQ10	Playa Espadilla West section	Quepos	444.65	371.90
AQ16	Playa Espadilla West section	Quepos	445.10	372.00
AQ19	Playa Macha	Quepos	444.92	374.20
AQ20	Playa Macha	Quepos	444.92	374.20
AQ22	Playa Macha	Quepos	444.92	374.20
AQ23	Playa Macha	Quepos	444.92	374.20
AQ28	Playa Macha	Quepos	444.92	374.20
AQ32	Playa Escondido	Quepos	448.25	370.25
AQ39	Playa between Esconido & Antonio	Quepos	448.05	369.90
AQ41	Playa between Esconido & Antonio	Quepos	448.05	369.90
AQ43	Playa Bizano	Quepos	445.80	372.55
AQ49	Playa Bizano	Quepos	445.80	372.55
AQ55	Playa Espadilla West section	Quepos	445.03	371.95
AQ62	Playa Manuel Antonia East section	Quepos	346.85	371.03
AQ66	Entrance Manuel Antonio	Quepos	346.88	371.12
AQ72	Playa Espadilla	Quepos	445.75	371.93
BQ28	near Park entrance	Quepos	446.85	370.88
BQ31	near Park entrance	Quepos	446.85	370.88
BQ32	near Park entrance	Quepos	446.85	370.88
BQ70	Playa Espadilla	Quepos	445.75	371.93
BQ71	Playa Espadilla	Quepos	445.75	371.93
BQ72	Playa Espadilla	Quepos	445.75	371.93
		Osa		
OS2	Road Carcarita-Rincon	Rincon	530.50	302.00
OS4	Isla Violin	Sierpe	501.70	305.20
OS6	Punta Ganado	Sierpe	502.40	298.90
OS9	Northern Osa Drake	Sierpe	502.10	302.60
OS16	Rio Tigre	Golfo Dulce	528.25	275.95

5.2.2. Nicoya, Herradura, Golfito, Burica (95–75 Ma): Caribbean LIP Basement

[24] The magmatism of these complexes is contemporaneous with widespread submarine volcanism recognized throughout the Caribbean plate and northwestern South America [*Sinton et al.*, 1998], generating oceanic crust of up to 15- to 20-km thickness [e.g., *Burke et al.*, 1978; *Maufrett and Leroy*, 1997; *Driscoll and Diebold*, 1998]. Therefore these volcanic successions are often referred to as a large

igneous province that produced a vast oceanic plateau [e.g., *Donnelly et al.*, 1990]. The magmatic peak activity occurred between 92 and 88 Ma [*Sinton et al.*, 1998] and is believed to coincide with the initiation of the Galápagos hotspot [*Duncan and Hargraves*, 1984] (see Figure 11b). Even though the lavas erupted over an area of $\sim 3 \times 10^6$ km^2 with a total volume of up to 4×10^6 km^3 [*Coffin and Eldholm*, 1993], the majority of lavas have strikingly uniform, flat incompatible element patterns (La/Yb = 0.92 ± 0.12, n = 64 out of 79, 2σ) and uniform initial Sr-Nd-Pb isotopic compositions (e.g., $(^{87}Sr/^{86}Sr)_{in}$ = 0.7034 ± 4, $(^{143}Nd/^{144}Nd)_{in}$ = 0.51291 ± 3, and $(^{206}Pb/^{204}Pb)_{in}$ = 18.86 ± 0.13, n = 54 out of 66, 2σ) [*Hauff et al.*, 2000]. The initial Sr-Nd-Pb isotope ratios completely overlap with the Galápagos field at 90 Ma and thus are at least consistent with a derivation from the Galápagos hotspot. The isotope and trace element data are interpreted to reflect the presence of recycled oceanic lithosphere in the source. The Sm-Nd and U-Pb isotope systematics further suggest relatively short recycling times of 300–500 myr; the time since the formation of the oceanic crust until melting to form the flood basalts at ~90 Ma [*Hauff et al.*, 2000].

[25] Since some Cretaceous Pacific MORBs that clearly formed away from mantle plumes have geochemical characteristics similar to those of the CLIP lavas [*Janney and Castillo*, 1997] it could be argued that the "plume-like" character of the CLIP is not exclusive to intraplate plateaus. However, the most feasible explanation for widespread volcanism throughout the Caribbean between 92 and 88 Ma is a starting plume head model. Moreover, seismic transects across the Central American land bridge image overthickened oceanic basement [*Stavenhagen et al.*, 1997; *Christeson et al.*, 1999; *Sallarès et al.*, 1999] with a velocity structure similar to the Ontong Java Plateau [*Gladczenko et al.*, 1997]. Therefore the Nicoya, Herradura, Golfito, and Burica seem to represent pieces of uplifted Caribbean oceanic plateau basement rather than accreted oceanic crust.

[26] A second magmatic pulse at ~75 Ma is recorded in the central Caribbean, Curaçao and western Colombia and is attributed to rifting of the overthickened plateau crust which in turn led to further upwelling and decompression melting of the underlying plume material [*Sinton et al.*, 1998]. Volcanism similar in composition to the 92–88 Ma flood basalts occurs in the Costa Rican complexes from 95 to 75 Ma (Nicoya, ~95–83 Ma; Herradura, 86–84 Ma; Golfito/Burica, >75 Ma). Northeastward migration of the oceanic plateau after its formation [*Duncan and Hargraves*, 1984] (see Figure 11b) would result in transport of the southwestern plateau margin over the (stationary) plume tail. This suggests that the plume stem produced magma continuously from ~95 to ~75 Ma. Paleomagnetic data of the Nicoya, Herradura, Golfito, and Burica complexes indicate an origin from equatorial latitudes [*Frisch et al.*, 1992] consistent with the location of the Galápagos hotspot. At ~80 Ma the northeastern margin of the plateau collided with the Greater Antilles Arc, causing a subduction reversal of the proto-Caribbean oceanic crust beneath the Greater Antilles and accretion of the oceanic plateau between the Americas [*Duncan and Hargraves*, 1984; *Pindell and Barrett*, 1990] (see Figure 11b). The implications of radiolarites exposed along the circum-Caribbean plateau margins, which have Pacific (central Tethian) faunal affinities and range in age from Pliensbachian to Santonian (195–84 Ma) [*Baumgartner*, 1984; *Montgomery et al.*, 1994a; *Schmidt-Effing*, 1979], are threefold. First, their paleo-environmental facies suggests that they represent deposits of a biosiliceous high pro-

ductivity zone located in the equatorial eastern Pacific [*Astorga*, 1997] (see Figure 11a). Second, their biostratigraphic age being partly older than the opening of the proto-Caribbean sea at ~165 Ma [e.g., *Pindell and Barrett*, 1990] strongly indicates a Pacific origin of large parts of the Caribbean plate through significant lateral transport [*Montgomery et al*., 1994b]. Third, the whereabouts of the preexisting oceanic crust onto which the radiolarites were deposited remain enigmatic. More detailed radiometric age dating of igneous especially in areas where they are closely associated with the radiolarites is necessary to detect the preexisting crust.

5.2.3. Tortugal (89 Ma): A unique source component within the CLIP or extent of the Chortis block south of the Hess Escarpment

[27] A single radiometric age date (89.7 ± 1.7 Ma) [*Alvarado et al*., 1997] suggests that magmatism at Tortugal is at least in part contemporaneous to Nicoya. Although the chemical composition of the Tortugal tholeiites is consistent with derivation from the CLIP source, the large differences in incompatible element concentrations and initial Sr-Nd-Pb isotope ratios require derivation of the alkaline volcanic rocks and picrites from a distinct source. Within the CLIP, Gorgona Island off the coast of Colombia (Figure 1) is the only known locality for the coexistence of spinifex-textured, chemically depleted komatiites, tholeiites with intermediate chemical composition, and chemically enriched transitional tholeiites [*Aitken and Echeverría*, 1984; *Dupré and Echeverría*, 1984; *Echeverría*, 1980]. In contrast to the Gorgona komatiites, the ultramafic rocks at Tortugal are olivine cumulates and enriched in their incompatible element and isotopic compositions. Even compared to the Gorgona transitional tholeiites, the Tortugal alkaline lavas have significantly higher incompatible concentrations and less radiogenic initial Nd and Pb isotopic compositions. The enriched Tortugal melts must therefore originate from a distinct source yet unknown within the CLIP. Similarities in trace element (Figure 5b) and isotopic compositions (Figures 9 and 10) between alkaline rocks from Santa Elena and Tortugal are, however, remarkable and suggest that they may originate from a common source and are both part of the Chortis block. These observations support geophysical evidence that the actual boundary between the Chortis block and the Chorotega block may lie south of the Hess Escarpment [*Goedde*, 1999] (see Figures 2 and 11d). This interpretation implies that the Nicoya Peninsula moved northward along a trench-parallel right lateral fault into its present location west of Tortugal [*Goedde*, 1999] (see Figures 2 and 11d). Because our preferred tectonic models require formation of the CLIP distant from the Chortis block, the presence of CLIP-type tholeiites at Tortugal is intriguing. In conclusion, the structural and age relationships of the magmatic series at Tortugal require better constraints.

5.2.4. Quepos and Osa (65–59 Ma): Accreted Galápagos paleo-hotspot track

[28] Formation of the Quepos and Osa magmatic complexes (65–59 Ma) occurred after the onset of Costa Rican arc volcanism in the late Campanian through Late Maastrichtian (74–65 Ma) [e.g., *Baumgartner et al*., 1984], thought to reflect northeastward subduction of Pacific lithosphere beneath thickened CLIP lithosphere [*Duncan and Hargraves*, 1984] (see Figure 11c). The OIB-like chemistry of the Quepos lavas and volcanological evidence for subaerial volcanism are consistent with an origin as an ocean island volcano [*Hauff et al*., 1997]. High $^3He/^4He$ ratio, ~12 times higher than the atmospheric ratio, in olivine mineral separates of picrites from Quepos indicate a deep mantle origin [*Hauff et al*., 2000] and are

characteristic for only a few hotspots such as Iceland and Galápagos [*Graham et al.*, 1993]. The majority of Osa lavas have incompatible element concentrations and initial Nd and Pb isotopic compositions similar to the CLIP basalts and to the lavas from the Cocos, Carnegie, and Coiba ridges (forming part of the Neogene Galápagos hotspot tracks), suggesting derivation from a common source. Depleted signatures in some Osa lavas most likely reflect the involvement of a depleted upper mantle component, possibly reflecting entrainment of asthenosphere into the plume by lithospheric shear as proposed for the present Galápagos plume [*White et al.*, 1993].

[29] Even though Quepos and Osa formed synchronously, important differences exist in their volcanic facies. While Quepos lavas partly erupted subaerially, emplacement of the Osa lavas seems to be exclusively submarine, probably above the carbonate compensation depth [*Berrangé and Thorpe*, 1988]. These differences could reflect formation of both structures as ocean island and aseismic ridge, respectively, over the subsequent tail of the Caribbean starting plume head [*Hauff et al.*, 1997], and imply that Osa and Quepos are part of the Galápagos paleo-hotspot track accreted to the Central American margin (Figure 11c). The spatial distribution and age relations of the Osa and Quepos complexes are remarkably similar to those of the aseismic Cocos ridge and seamounts to the northwest of the ridge, which represent drowned ocean islands presently being subducted off the coast of Costa Rica [*von Huene et al.*, 1995; *Werner et al.*, 1999]. These structures also overlap in age (13.0–14.5 Ma) and show similar variations in geochemistry and volcanology [*Hoernle et al.*, 2000; *Werner et al.*, 1999], as observed for Quepos and Osa.

[30] Overlying mid-Eocene (49–41 Ma) olisthostromes at Quepos and the presence of a mid-Eocene through Miocene accretionary wedge on the trenchward side of the Osa Peninsula (Figure 2) confine the age of accretion to be mid-Eocene (Figure 11d). A regional early to late Oligocene (34–28 Ma) unconformity in the sedimentary basins of the Costa Rican Arc has been attributed to a large-scale deformation event [e.g., *Sprechmann et al.*, 1994], which occurred after the inferred arrival of the Osa/Quepos hotspot track at the Central American trench. These volcanic structures most likely formed morphological obstacles that caused deformation of the upper plate upon subduction [*Cloos*, 1993], similar to the presently subducting seamounts off the coast of Costa Rica and the collision of the Cocos ridge 5–7 myr ago [e.g., *De Boer et al.*, 1995; *von Huene et al.*, 1995]. Finally, accreted Paleogene seamount/ocean island complexes in western Panama [*Hoernle et al.*, 1998] seem to represent the missing temporal link between the Galápagos hotspot and the CLIP and testify to the continuous interaction of the Central American plate margin with the Galápagos hotspot track, influencing the tectonic, magmatic, and sedimentary evolution of this region.

6. Conclusions

[31] Laser $^{39}Ar/^{40}Ar$ age dating combined with a detailed study of major and trace element and initial Sr-Nd-Pb isotopic compositions of eight oceanic basement complexes in Costa Rica show the following:

1. Igneous rocks on the Santa Elena Peninsula (125–109 Ma) are the oldest radiometrically dated rocks in Costa Rica. The geochemistry of these tholeiitic rocks (Units II, III, and IV) indicates a subduction zone origin through melting of a Pacific MORB-type mantle wedge of the Chortis subduction zone, formerly located in front of Mexico. The alkaline rocks

(Unit I) have geochemical characteristics consistent with derivation through intraplate or OIB-type volcanism.

2. The majority of the Costa Rican igneous basement complexes (Nicoya, Herradura, the tholeiitic unit of Tortugal, Golfito, and Burica) formed over a relatively short time period (95–74 Ma), in sharp contrast to the extensive biostratigraphic record of radiolarian charts (164–84 Ma), which are intruded by or in fault contact with the 95–74 Ma igneous rocks. The similarity in age and geochemistry to other circum-Caribbean basement exposures provides evidence that these complexes are part of the Caribbean Large Igneous Province (CLIP). Magmatism in Costa Rica occurred continuously between the major phases of volcanic activity at circa 90 and 74 Ma, previously identified in other portions of the CLIP, consistent with northeastward migration of the oceanic plateau over a continuously active plume tail. More age dating, however, is required to fully constrain the temporal evolution of the oceanic plateau and to date the igneous portion of preexisting oceanic crust, which could be as old as 164 Ma on the basis of the ages of the radiolarites.
3. The remarkable trace element and isotopic similarities between the alkaline and picritic rocks from Tortugal and the alkali basalts from Santa Elena (Unit I) suggest a common origin and suggest that the structural boundary between the Chortis block and the Chorotega block may lie south of the Hess Escarpment.
4. The Quepos ocean island and Osa aseismic ridge complexes are believed to form part of the early Galápagos hotspot track (65–59 Ma). Accretion of the Quepos and Osa volcanic structures in the mid-Eocene may have caused large-scale regional deformation and uplift of the Central American Arc similar to the indenture of the Cocos ridge ~5 myr ago.

Acknowledgments

[32] Reviews by Bob Duncan, Pat Castillo, and Barry Hanan helped to improve the earlier version of this article. Overall support of this project by G. Tilton and H.-U Schmincke is gratefully acknowledged. J. Bryce and E. Zuleger assisted with the TIMS analyses, Kerstin Wolff and Volker Zöllmer assisted with the XRF and Jan Sticklus assisted with the laser Ar/Ar analyses. This study has been supported by the Deutsche Forschungsgemeinschaft (DFG) within the TICOSECT project (Trans Isthmus Costa Rican Transect). The German Academic Exchange Service (DAAD) granted F.H. a scholarship to carry out initial isotope studies at UCSB for his Ph.D.

References

Aitken, B. G., and L. M. Echeverría, Petrology and geochemistry of komatiites and tholeiites from Gorgona island, Colombia, *Contrib. Mineral. Petrol.*, *86*, 94–105, 1984.

Alvarado, G. E., and P. Denyer, Implications of the high-Mg mesozoic volcanic rocks in Costa Rica for the Caribbean region: The case of the Tortugal komatiite-like suite, *Z. Geol. Palaeontol.*, *Teil I, 3–6*, 409–429, 1998.

Alvarado, G. E., S. Kussmaul, S. Chiesa, P.-Y. Gillot, H. Appel, G. Wörner, and C. Rundle, Resumen cronostratigráfico de las rocas ígneas de Costa Rica basado en dataciones radiométricas K-Ar y U-Th, *J. South Am. Earth Sci.*, *6*(3), 151–168, 1992.

Alvarado, G. E., P. Denyer, and C. W. Sinton, The 89 Ma Tortugal komatiitic suite, Costa Rica: Implications for a common origin of the Caribbean and Eastern Pacific region from a mantle plume, *Geology*, *25*(5), 439–442, 1997.

Astorga, A., Descubrimiento de corteza oceanica mesozoica en el Norte de Costa Rica y el Sur de Nicaragua, *Rev. Geol. Am. Cent.*, *14*, 109–112, 1992.

Astorga, A., El puente-istmo de América Central y la evolución de la place Caribe (con énfasis en el Mesozico), *Profil*, *12*, 1–201, 1997.

Azéma, J., and J. Tournon, La péninsule de Santa Elena, Costa Rica: Un massif ultrabasique charríen marge pacifique de l'Amérique centrale, *C. R. Acad. Sci. Paris*, *290*, 9–12, 1980.

Azéma, J., and J. Tournon, The Guatemalan margin, the Nicoya Complex, and the origin of the Caribbean plate, *Initial Rep. Deep Sea Drill. Proj.*, *67*, 1982.

Baumgartner, P. O., El complejo ofíolitico de Nicoya (Costa Rica): Modelos estructurales analizados en función de las edades de los radiolarios (Calloviense a

Santoniense), in *Manual de Geología de Costa Rica*, edited by P. Sprechmann, pp. 115–123, Universidad de Costa Rica, Vol. (1), San José, 1984.

Baumgartner, P. O., C. R. Mora, B. J. J. Sigal, G. Glacon, J. Azéma, and J. Bourgois, Sedimentación y paleogeografía del Cretácico y Cenozoico del litoral Pacífico de Costa Rica, *Rev. Geol. Am. Cent.*, *1*, 57–136, 1984.

Bellon, H., and J. Tournon, Contribution de la géochronométrie K-Ar à l'étude du magmatism de Costa Rica, Amérique Central, *Bull. Soc. Geol. Fr.*, *6*(7), 955–959, 1978.

Berrangé, J. P., and R. S. Thorpe, The geology, geochemistry and emplacement of the Cretaceous-tertiary ophiolitic Nicoya complex of the Osa Peninsula, southern Costa Rica, *Tectonophysics*, *147*, 193–220, 1988.

Berrangé, J. P., D. R. Bradley, and N. J. Snelling, K/Ar dating of the ophiolitic Nicoya Complex of the Osa Peninsula, southern Costa Rica, *J. South Am. Earth Sci.*, *2*(1), 49–59, 1989.

Bogaard, P. V. D., $^{40}Ar/^{39}Ar$ of sanidine phenocrysts from Laacher See tephra (12.900 yr BP): Chronostratigraphy and petrological significance, *Earth Planet. Sci. Lett.*, *133*, 163–174, 1995.

Burke, K., P. J. Fox, and A. M. C. Sengör, Buoyant ocean floor and the evolution of the Caribbean, *J. Geophys. Res.*, *83*, 3949–3954, 1978.

Chaffey, D. J., R. A. Cliff, and B. M. Wilson, Characterization of the St Helena magma source, in *Magmatism in the Ocean Basins*, edited by A. D. Saunders and M. J. Norry, *Geol. Soc. London Spec. Publ.*, *42*, 257–276, 1989.

Christeson, G. L., K. D. McIntosh, T. H. Shipley, E. R. Flueh, and H. Goedde, Structure of the Costa Rica convergent margin, offshore Nicoya Peninsula, *J. Geophys. Res.*, *104*(B11), 25,443–25,468, 1999.

Cloos, M., Lithospheric buoyancy and collisional orogenesis: Subduction of oceanic plateaus, continental margins, island arcs, spreading ridges, and seamounts, *Geol. Soc. Am. Bull.*, *105*, 715–737, 1993.

Coffin, M. F., and O. Eldholm, Scratching the surface: Estimating dimensions of large igneous provinces, *Geology*, *21*, 515–518, 1993.

De Boer, J. Z., M. S. Drummond, M. J. Bordelon, M. J. Defant, H. Bellon, and R. C. Mauri, Cenozoic magmatic phases of the Costa Rican island arc (Cordillera de Talamanca), in *Geologic and Tectonic Development of the Caribbean Plate Boundary in Southern Central America*, vol. 295, edited by P. Mann, pp. 35–55, Geol. Soc. of Am., Boulder, Colo., 1995.

DeWever, P., J. Azéma, J. Tournon, and A. Desmet, Découverte de matérial océanique du Lias-Dogger inférireur dans la péninsule de Santa Elena (Costa Rica, Amérique Centrale), *C. R. Acad Sci. Paris, Ser. II*, *300*(15), 759–764, 1985.

Di Marco, G., Les terrains accrétés du sud du Costa Rica. Évolution tectonostratigraphic de la marge occidentale de la plaque Caraibe., Ph.D. thesis, Univ. de Lausanne, Lausanne, France, 1994.

Donnelly, T. W., D. Beets, M. J. Carr, T. Jackson, G. Klavier, J. Lewis, R. Maury, H. Schellenkens, A. L. Smith, G. Wadge, and D. Westercamp, History and tectonic setting of Caribbean magmatism, in *The Caribbean Region* vol. H, *The Geology of North America*, edited by G. Dengo and J. E. Case, pp. 339–374, Geol. Soc. of Am., Boulder, Colo., 1990.

Driscoll, N. W., and J. B. Diebold, Deformation of the Caribbean region: One plate or two?, *Geology*, *26*, 1043–1046, 1998.

Duffield, W. A., and G. B. Dalrymple, The Taylor Creek Rhyolite of New Mexico; a rapidly emplaced field of lava domes and flows, *Bull. Volcanol.*, *52*, 475–487, 1990.

Duncan, R. A., and R. B. Hargraves, Caribbean region in the mantle reference frame, in *The Caribbean-South American Plate Boundary and Regional Tectonics*, edited by W. Bonini, R. B. Hargraves, and R. Shagam, *Mem. Geol. Soc. Am.*, *162*, 89–121, 1984.

Dupré, B., and L. M. Echeverría, Pb isotopes of Gorgona island (Colombia): Isotope variations correlated with magma type, *Earth Planet. Sci. Lett.*, *67*, 186–190, 1984.

Echeverría, L. M., Tertiary or Mesozoic komatiites from Gorgona island, Colombia: Field relations and geochemistry, *Contrib. Mineral. Petrol.*, *73*, 253–266, 1980.

Elliot, T., T. Plank, A. Zindler, W. White, and B. Bourdon, Element transport from slab to volcanic front at the Mariana arc, *J. Geophys. Res.*, *102*, 14,991–15,019, 1997.

Flüh, E., The basic igneous complex - Trace of an ancient Galápagos hot spot aseismic ridge?, *Z. Geol. Palaeontol.*, *Teil 1*, 3/4, 291–303, 1983.

Frisch, W., M. Meschede, and M. Sick, Origin of the Central American ophiolites: Evidence from paleomagnetic results, *Geol. Soc. Am. Bull.*, *104*, 1301–1314, 1992.

Galli-Olivier, C., Ophiolite and island arc volcanism in Costa Rica, *Geol. Soc. Am. Bull.*, *90*, 444–452, 1979.

Garbe-Schönberg, C.-D., Simultaneous determination of thirty-seven trace elements in twenty-eight international rock standards by ICP-MS, *Geostand. Newsl.*, *17*, 81–97, 1993.

Gladczenko, T. Z., M. F. Coffin, and O. Eldholm, Crustal structure of the Ontong Java Plateau: Modelling of new gravity and existing seismic data, *J. Geophys. Res.*, *102*, 22,711–22,729, 1997.

Goedde, H., Die Krustenstrukturen am konvergenten Plattenrand im Norden Costa Ricas; Refraktionsseismische

Messungen und ihre geologisch-geodynamische Interpretation, *Tech. Sci. Rep. STR 99/17*, GFZ-Potsdam, Germany, 1999.

Govindaraju, K., Compilation of working values and sample descriptions for 383 geostandards, *Geostand. Newsl.*, *18*, special issue, 158 pp., 1994.

Gradstein, F. M., and J. G. Ogg, A Phanerozoic time scale, *Episodes*, *19*, 3–5, 1996.

Graham, D. W., D. M. Christie, K. S. Harpp, and J. E. Lupton, Mantle plume helium in submarine basalts from the Galápagos Platform, *Science*, *262*(5142), 2023–2026, 1993.

Hart, S. R., A large-scale isotope anomaly in the Southern Hemisphere mantle, *Nature*, *309*, 753–757, 1984.

Hauff, F., K. Hoernle, H.-U. Schmincke, and R. Werner, A mid Cretaceous origin for the Galápagos hotspot: Volcanological, petrological, and geochemical evidence from Costa Rican oceanic crustal segments, *Geol. Rundsch.*, *86*, 141–155, 1997.

Hauff, F., K. Hoernle, G. Tilton, D. Graham, and A. C. Kerr, Large volume recycling of oceanic lithosphere over short time scales: Geochemical constraints from the Caribbean Large Igneous Province, *Earth Planet. Sci. Lett.*, *174*, 247–263, 2000.

Hein, J. R., E. Kuijpers, P. Denyer, and R. Sliney, Petrology and geochemistry of Cretaceous and Paleogene charts from Western Costa Rica, in *Siliceous Deposits in the Pacific Region*, vol. 36, edited by A. Iijima, J. R. Hein, and R. Siever, pp. 143–174, Elsevier, New York, 1983.

Hoernle, K. A., and G. R. Tilton, Sr-Nd-Pb isotope data for Fuerteventura (Canary Islands) basal complex and subaerial volcanics: Applications to magma genesis and evolution, *Schweiz. Mineral. Petrogr. Mitt.*, *71*, 3–18, 1991.

Hoernle, K., U. Schweikert, R. Werner, and P. van den Bogaard, The Caribbean flood basalt event and the missing link the Galápagos hotspot: Preliminary results from Panama, *Terra Nostra*, *5*, 69, 1998.

Hoernle, K., R. Werner, J. Phipps Morgan, J. Bryce, and J. Mrazek, Existence of a complex spatial zonation in the Galápagos plume for at least 14.5 Ma, *Geology*, in press, 2000.

Hofmann, A. W., Chemical differentiation of the Earth: The relationship between mantle, continental and oceanic crust, *Earth Planet. Sci. Lett.*, *90*, 297–314, 1988.

Janney, P. E., and P. R. Castillo, Geochemistry of Mesozoic Pacific mid-ocean ridge basalt: Constraints on melt generation and the evolution of the Pacific upper mantle., *J. Geophys. Res.*, *102*, 5207–5229, 1997.

Jochum, K.-P., H. M. Seufert, and M. F. Thirlwall, Multi-element analyses of 15 international standard rocks by isotope dilution spark source mass spectrometry, *Geostand. Newsl.*, *14*, 469–473, 1990.

Kerr, A. C., J. Tarney, G. F. Marriner, A. Nivia, and A. D. Saunders, The Caribbean-Colombian Igneous Province: The internal anatomy of an oceanic plateau, in *Large Igneous Provinces, Geophys. Monogr. Ser.*, vol. 100, edited by J. J. Mahoney and M. F. Coffin, pp. 123–144, AGU, Washington, D. C., 1997.

Kerr, A. C., M. A. Iturralde-Vinent, A. D. Saunders, T. L. Babbs, and J. Tarney, A new plate tectonic model of the Caribbean: Implications from a geochemical reconnaissance of Cuban Mesozoic volcanic rocks, *Geol. Soc. Am. Bull.*, *111*, 1581–1599, 1999.

Le Maitre, R. W., *A Classification of Igneous Rocks and Glossary of Terms*, 193 pp., Blackwell Sci., Malden, Mass., 1989.

Macdonald, G. A., and T. Katsura, Chemical composition of Hawaiian lavas, *J. Petrol.*, *5*, 82–133, 1964.

Mahoney, J. J., M. Storey, R. A. Duncan, K. J. Spencer, and M. Pringle, Geochemistry and age of the Ontong Java Plateau, in *The Mesozoic Pacific: Geology, Tectonics and Volcanism, Geophys. Monogr. Ser.*, vol. 77, edited by M. S. Pringle et al., pp. 233–261, AGU, Washington, D. C. 1993.

Maufrett, A., and S. Leroy, Seismic stratigraphy and structure of the Caribbean igneous province, *Tectonophysics*, *293*, 61–104, 1997.

Meschede, M., and W. Frisch, A plate tectonic model for the Mesozoic and Early Cenozoic history of the Caribbean plate, *Tectonophysics*, *296*, 269–291, 1998.

Montgomery, H., E. A. Pessagno, J. F. Lewis, and J. Schellekins, Paleogeography of Jurassic fragments in the Caribbean, *Tectonics*, *13*, 725–732, 1994a.

Montgomery, H., E. A. Pessagno, and J. L. Pindell, A 195 Ma terrane in 165 Ma sea: Pacific origin of the Caribbean plate, *GSA Today*, *4*, 3–7, 1994b.

Neal, C. R., J. J. Mahoney, L. W. Kroenke, R. A. Duncan, and M. G. Petterson, The Ontong Java Plateau, in *Large Igneous Provinces*, edited by J. J. Mahoney and M. F. Coffin, *Geophys. Monogr. Ser.*, vol. 100, pp. 183–216, AGU, Washington, D. C., 1997.

Pindell, J. L., and S. F. Barrett, Geological evolution of the Caribbean region; a plate tectonic perspective, in *The Caribbean Region*, vol. H, *The Geology of North America*, edited by G. Dengo and J. E. Case, pp. 405–432, Geol. Soc. of Am., Boulder, Colo., 1990.

Sallarès, V., J. J. Dañobeitia, E. R. Flueh, and G. Leandro, Seismic velocity structure across the Middle American landbridge in Northern Costa Rica, *J. Geodyn.*, *27*, 327–344, 1999.

Schmidt-Effing, R., Alter und Genese des Nicoya-Komplexes, einer ozeanischen Paläokruste (Oberjura bis Eozän) im südlichen Zentralamerika, *Geol. Rundsch.*, *68*(H.2), 457–494, 1979.

Schmidt-Effing, R., Radiolarien der Mittel-Kreide aus dem Santa Helena Massiv von Costa Rica, *Neues Jahrb. Geol. Palaeontol. Abh.*, *160*(2), 241–257, 1980.

Seyfried, H., and P. Sprechmann, Acerca de la formación del puente-istmo centroamericano meridional, con énfasis en el desarollo acaecido desde el Campaniense al Eoceno, *Rev. Geol. Am. Cent.*, *2*, 63–87, 1985.

Sinton, C. W., R. A. Duncan, and P. Denyer, Nicoya Peninsula, Costa Rica: A single suite of Caribbean oceanic plateau magmas, *J. Geophys. Res.*, *102*(B7), 15,507–15,520, 1997.

Sinton, C. W., R. A. Duncan, M. Storey, J. Lewis, and J. J. Estrada, An oceanic flood basalt province within the Caribbean plate, *Earth Planet. Sci. Lett.*, *155*, 221–235, 1998.

Sprechmann, P., A. Astorga, C. Calvo, and A. Fernández, Stratigraphic chart of the sedimentary basins of Costa Rica, Central America, *Profil*, *7*, 427–433, 1994.

Stavenhagen, A. U., E. R. Flueh, C. Ranero, K. D. McIntosh, T. Shipley, G. Leandro, A. Schulze, and J. J. Dañobeitia, Seismic wide-angle investigations in Costa Rica - A crustal velocity model from the Pacific to the Caribbean coast, *Z. Geol. Palaeontol.*, *Teil I, 3–6*, 393–408, 1997.

Storey, M., M. S. Pringle, M. F. Coffin, and J. Wijbrims, Geochemistry and geochronology of Kerguelen Plateau basalts: Results from ODP Legs 119 and 120, *Eos Trans. AGU*, *76*, W123, 1996.

Sun, S.-S., and W. F. McDonough, Chemical and isotopic systematics of oceanic basalts: Implications for mantle composition and processes, in *Magmatism in the Ocean Basins*, edited by A. D. Saunders and M. J. Norry, *Geol. Soc. London Spec. Publ.*, *42*, 313–345, 1989.

Thirlwall, M. F., Pb isotopic and elemental evidence for OIB derivation from young HIMU mantle, *Chem. Geol.*, *139*, 51–74, 1997.

Todt, W., R. A. Cliff, A. Hanser, and A. W. Hoffman, Evaluation of a ^{202}Pb-^{205}Pb double spike for high precision lead isotope analyses, in *Earth Processes: Reading the Isotopic Code*, edited by A. Basu and S. Hart, *Geophys. Monogr. Ser.*, vol. 95, pp. 429–437, AGU, Washington, D. C., 1996.

Tournon, J., The Santa Elena Peninsula: An ophiolitic nappe and a sedimentary volcanic relative autochthonous, *Profil*, *7*, 87–96, 1994.

Tournon, J., and G. E. Alvarado, *Carte géologique du Costa Rica/Mapa geológico de Costa Rica*, 79 pp., Instit. Tecnol. de Costa Rica, Catargo, 1997.

Tournon, J., M. Seyler, and A. Astorga, Les péridotites du Rio San Juan (Nicaragua et Costa Rica) jalons possibles d'une suture ultrabasique E-W en Amérique Centrale méridionale, *C. R. Acad Sci. Paris, Ser. IIa*, *320*, 757–764, 1995.

von Huene, R., E. Bialas, E. Flüh, B. Cropp, T. Csernok, E. Fabel, J. Hoffmann, K. Emeis, P. Holler, G. Jeschke, C. Leandro, I. Peréz Fernandéz, S. Chavarria, A. Florez, Z. Escobedo, R. León, and O. Barrios, Morphotectonics of the Pacific convergent margin of Costa Rica, in *Geologic and Tectonic development of the Caribbean Plate Boundary in Southern Central America*, edited by P. Mann, *Geol. Soc. Am. Spec. Pap.*, *295*, 291–307, 1995.

Werner, R., K. Hoernle, P. van den Bogaard, C. Ranero, R. von Huene, and D. Korich, A drowned 14 Ma old Galápagos Archipelago off the coast of Costa Rica: Implications for evolutionary and tectonic models, *Geology*, *27*, 499–502, 1999.

White, W. M., A. R. McBirney, and R. A. Duncan, Petrology and geochemistry of the Galápagos Islands: Portrait of a pathological mantle plume, *J. Geophys. Res.*, *98*(B11), 19,533–19,563, 1993.

York, D., Least squares fitting of a straight line with correlated errors, *Earth Planet. Sci. Lett.*, *5*, 320–324, 1969.